JETP Letters, Vol. 81, No. 5, 2005, pp. 201–204. Translated from Pis'ma v Zhurnal Éksperimental'noĭ i Teoreticheskoĭ Fiziki, Vol. 81, No. 5, 2005, pp. 259–262.

Optical–Acoustic Soliton under the Conditions of Slow Light and Stimulated Mandelstam–Brillouin Scattering

S. V. Sazonov

Kaliningrad State University, Kaliningrad, 236041 Russia

e-mail: barab@newmail.ru

Received December 16, 2004

The possibility of forming a stable optical–acoustic soliton in the regime of electromagnetically induced transparency has been analyzed under the condition that the group velocity of light in a medium with stimulated Mandelstam–Brillouin scattering decreases to the speed of sound. This possibility exists because the forward Mandelstam–Brillouin scattering, which is forbidden in a nondispersive medium, is allowed under this condition. The optical component is an envelope pulse, and the acoustic component has no carrier frequency. It has been shown that such a soliton can be formed for anomalously low input intensities of the optical pulse. © *2005 Pleiades Publishing, Inc.*

PACS numbers: 42.50.Ar, 42.65.Es, 42.81.–i

Experimental advances in anomalously strong light slowing both in gases [1] and in solids [2] in the regime of electromagnetically induced transparency (EIT) stimulated a series of works on optical–acoustic interaction under the conditions of the collinear propagation of light and sound [3–5]. In this geometry, this interaction is most efficient when the group velocity of light is equal to the speed of sound in the substance under consideration. Soliton mechanisms of the generation of acoustic pulses in noncollinear regimes of optical–acoustic interaction were analyzed in [6]. The possibility of the hypersonic transparency of the absorbing paramagnetic by means of microwave electromagnetic radiation supplied to the sample perpendicularly to the propagation of the acoustic pulse was analyzed in [7]. The equality of the speeds of light and sound is not necessary in noncollinear geometry.

Matsko *et al.* [4] showed that the parameters of stimulated Mandelstam–Brillouin scattering (SMBS) change substantially when the group velocity of light approaches the speed of sound. In particular, they concluded that forward SMBS was possible under the conditions of strongly slowed light. This scattering in a nondispersive medium is forbidden by the conservation laws for energy and momentum in interactions between photons and phonons [8].

Since SMBS is a purely nonlinear effect, not only the effect of the acoustic phonon branch on light but also inverse action is important. At the same time, the medium slowing light is strongly dispersive. As is known, the presence of nonlinearity and dispersion can give rise to the formation of a soliton in such a medium. In view of this circumstance, a question arises as to whether the generation of an acoustic soliton is possible with its further synchronous propagation with the slowed light pulse in the regime of forward SMBS. This problem is studied in this work.

Let us consider a continuous isotropic medium (matrix) containing impurities with resonance three-level λ transitions. Intense optical pumping at the $2 \longleftrightarrow 3$ transition (quantum levels are enumerated from bottom to top) creates the EIT regime for a signal pulse that is much less intense and that is in resonance with the $1 \longleftrightarrow 3$ transition. The latter transition is characterized by a sharp decrease in the absorption coefficient (almost to zero) and group velocity of the signal pulse, as well as by the trapping of the populations of quantum levels in the system of λ transitions.

The polarization response $P(\mathbf{r}, t)$ of the dispersive medium to the action of the linearly polarized signal field $E(\mathbf{r}, t)$ is represented in the form

$$P(\mathbf{r}, t) = \chi_m E(\mathbf{r}, t) + \int_0^\infty \chi(\tau) E(\mathbf{r}, t-\tau) dT, \qquad (1)$$

where χ_m is the dielectric susceptibility of the matrix, which is assumed to be nondispersive in the frequency range under consideration, and $\chi(\tau)$ is the susceptibility of the dispersive medium of three-level impurity atoms.

The acoustic phonon branch leads to the modulation of the matrix susceptibility [8]:

$$\chi_m = \chi_m^{(0)} + (\partial \chi_m / \partial u)_0 u, \qquad (2)$$

where $u(\mathbf{r}, t)$ is the field of local longitudinal deformations of the medium and the subscript 0 corresponds to the absence of strains.

0021-3640/05/8105-0201$26.00

Under these conditions, the energy density of optical–acoustic interaction that is associated with SMBS has the form

$$V_{\text{int}} = -\frac{1}{2}\left(\frac{\partial\chi_m}{\partial u}\right)_0 uE^2. \quad (3)$$

The Hamiltonian density for the acoustic field has the form

$$V_a = \frac{p^3}{2\rho_m} + \frac{1}{2}\rho_m a^2(\nabla s)^2, \quad (4)$$

where ρ_m is the average density of the medium; a is the speed of longitudinal sound in it; s is the local displacement field that is related to the strain field as $u = \partial s/\partial z$, where the z axis coincides with the direction of the propagation of the optical pulse and acoustic pulse that is generated by the optical pulse; and p is the field of the momentum density of local displacements. Using Eqs. (3) and (4) and the Hamiltonian equations for the continuous medium

$$\frac{\partial s}{\partial t} = \frac{\delta H}{\delta p}, \quad \frac{\partial p}{\partial t} = -\frac{\delta H}{\delta s},$$

where $H = \int (V_a + V_{\text{int}})\, d^3\mathbf{r}$, we obtain

$$\Delta u - \frac{1}{a^2}\frac{\partial^2 u}{\partial t^2} = \frac{1}{2\rho_m a^2}\left(\frac{\partial\chi_m}{\partial u}\right)_0 \frac{\partial^2}{\partial z^2}(E^2), \quad (5)$$

where Δ is the Laplace operator.

Using Eqs. (1) and (2) and Maxwell equations for E, we arrive at the equation

$$\Delta E - \frac{n_m^2}{c^2}\frac{\partial^2 E}{\partial t^2} = \frac{4\pi}{c^2}\frac{\partial^2}{\partial t^2}\left[\int_0^\infty \chi(\tau)E(\mathbf{r}, t-\tau)d\tau + \left(\frac{\partial\chi_m}{\partial u}\right)_0 uE\right], \quad (6)$$

where c is the speed of light in vacuum and $n_m = \sqrt{1 + 4\pi\chi_m}$ is the refractive index of the matrix. The nonlinear integro-differential system of Eqs. (5) and (6) self-consistently describes the SMBS regime in the dispersive medium.

Let us consider a light field in the form of a quasi-monochromatic pulse with carrier frequency ω_0 and wavenumber k_0. In this case,

$$E(\mathbf{r}, t) = \psi(\mathbf{r}, t)\exp[i(\omega_0 t - k_0 z)] + \text{c.c.}, \quad (7)$$

where $\psi(\mathbf{r}, t)$ is the slowly varying envelope. Following [9], we substitute Eq. (7) into Eq. (6) and expand $\psi(\mathbf{r}, t-\tau)$ in a Taylor series in τ. Taking into account only minimum-order group dispersion, we write

$$\int_0^\infty \chi(\tau)E(\mathbf{r}, t-\tau)d\tau = \left[\chi(\omega_0)\psi - i\left(\frac{\partial\chi}{\partial\omega}\right)\frac{\partial\psi}{\partial t} - \frac{1}{2}\left(\frac{\partial^2\psi}{\partial\omega^2}\right)_0\frac{\partial^2\psi}{\partial t^2}\right] \times \exp[i(\omega_0 t - k_0 z)] + \text{c.c.}, \quad (8)$$

where $\chi(\omega) = \int_0^\infty \chi(\tau)\exp(i\omega\tau)d\tau$ is the frequency susceptibility of impurities and the subscript 0 means that the corresponding derivatives are calculated at $\omega = \omega_0$.

Substituting Eqs. (7) and (8) into Eqs. (6) and (5) and ignoring relatively fast-oscillating terms, we obtain

$$i\left(\frac{\partial\psi}{\partial z} + \frac{1}{v_g}\frac{\partial\psi}{\partial t}\right) + \frac{k_2}{2}\frac{\partial^2\psi}{\partial t^2} = \frac{2\pi\omega_0}{cn}\left(\frac{\partial\chi_m}{\partial u}\right)_0 u\psi + \frac{c}{2n\omega_0}\Delta_\perp\psi, \quad (9)$$

$$\frac{\partial^2 u}{\partial z^2} - \frac{1}{a^2}\frac{\partial^2 u}{\partial t^2} = \frac{1}{\rho_m a^2}\left(\frac{\partial\chi_m}{\partial u}\right)_0\frac{\partial^2}{\partial z^2}(|\psi|^2) - \Delta_\perp u, \quad (10)$$

respectively. Here, $\psi_g = c/(n + \omega_0(\partial n/\partial\omega)_0)$ is the group velocity of the optical signal pulse, $n = [1 + 4\pi(\chi_m + \chi(\omega_0))]^{1/2}$ is the total refractive index of the medium, $k_2 = (\partial(1/v_g)/\partial\omega)_0$ is the dispersion parameter for the group velocity, and $\Delta_\perp$ is the transverse Laplacian. Note that, in contrast to the optical field, the acoustic wave is represented in Eqs. (9) and (10) by the strain field rather than the envelope. Therefore, the acoustic pulse generally has no the carrier frequency.

In what follows, the carrier frequency ω_0 of the optical signal pulse is assumed to be exactly equal to the frequency of the $1 \longleftrightarrow 3$ quantum transition. In this case, $\chi(\omega_0) = 0$ [10] and $(\partial^2 n/\partial\omega^2)_0 = 0$ [11] and, therefore, $n = n_m$ and $k_2 = 2(\partial n/\partial\omega)_0/c > 0$. Thus, the group dispersion at the center of the resonance absorption line is positive.

For the one-dimensional case ($\Delta_\perp = 0$), Eqs. (9) and (10) transform into the known Zakharov system [12]. For $v_g = a$, the Zakharov–Benni resonance or resonance of long and short waves [13] is realized: the group velocity of the short-wavelength (optical) component is equal to the phase velocity of the long-wavelength (acoustic) component. This is the condition under which the interaction between sound and slowed light is most efficient. In this case, it is convenient to analyze Eq. (10) in the approximation of quasi-unidirectional propagation [13]. Since Eq. (2) is an expansion, the first term on the right-hand side of Eq. (10) is small. In addition, the paraxial approximation is used ($\Delta_\perp u \ll$

$\partial^2 u/\partial z^2$). Introducing the "local" time $\tau = t - z/a = t - z/v_g$ and the "slow" coordinate $\zeta = \mu z$, where the small parameter μ is proportional to the right-hand side of Eq. (10), and ignoring $\sim\mu^2$ terms, we represent Eqs. (9) and (10) in the form

$$i\frac{\partial\psi}{\partial z} + \frac{k_2}{2}\frac{\partial^2\psi}{\partial\tau^2} = \alpha u\psi + \frac{c}{2n_m\omega_0}\Delta_\perp\psi, \tag{11}$$

$$\frac{\partial u}{\partial z} = -\beta\frac{\partial}{\partial\tau}(|\psi|^2) + \frac{a}{2}\Delta_\perp\int_{-\infty}^{\tau} u d\tau', \tag{12}$$

where $\alpha = (2\pi\omega_0/cn)(\partial\chi_m/\partial u)_0$ and $\beta = (\partial\chi_m/\partial u)_0/(2\rho_m a^3)$.

In the one-dimensional case, Eqs. (11) and (12) present the integrable Yadjima–Oikawa system [14], which has the single-soliton solution

$$\psi = \psi_m e^{-i(\Omega t - qz)}\operatorname{sech}\left(\frac{t - z/V}{\tau_p}\right),$$
$$u = -u_m\operatorname{sech}^2\left(\frac{t - z/V}{\tau_p}\right). \tag{13}$$

Here, $\psi_m = (|k_2|/\tau_p)\sqrt{\Omega/\alpha\beta}$, $u_m = k_2/\alpha\tau_p^2$, $q = \Omega/a + (k_2/2)(1/\tau_p^2 - \Omega^2)$, and the propagation velocity V is determined by the relation $1/V = 1/a - k_2\Omega$.

Solution (13) involves two free parameters, namely, the duration τ_p and the nonlinear shift Ω of the optical component of the soliton. It follows from the expressions for α, β, and ψ_m that $\Omega \geq 0$. According to this relation and Eqs. (13) and (7), we conclude that the frequency of the optical component is shifted toward the red spectral range: $\omega_0 \longrightarrow \omega_0 - \Omega$. This corresponds to a decrease in the energy of each photon undergoing SMBS and to the excitation of phonon modes.

As follows from [4], for $v_g = a$ and forward scattering there are no formal constraints on Ω. However, note that Ω has an upper limit because (i) the envelope ψ varies slowly and thereby $\Omega \ll \omega_0$ [see Eqs. (7) and (13)] and (ii) the Ω value must correspond to the dispersionless approximation accepted here for sound and, hence, to the low-frequency range of the first Brillouin zone. For this reason, there is a lower limit for the pulse duration: $\tau_p \gg h/a$, where h is the distance between elementary cells (nearest neighbors) in the medium in the soliton propagation direction. Setting $h \approx 5\times10^{-8}$ cm and $a \approx 5\times10^5$ cm/s, we obtain $\tau_p \gg 10^{-13}$ s. Thus, the lower limit is $\tau_p \sim 1$ ps.

Note that, at $\Omega = 0$, the optical component of the soliton vanishes; i.e., the entire energy of the input light pulse is transformed to the strain soliton. In order to reveal the conditions under which this phenomenon is possible, it is necessary to solve the boundary value problem for the system of Eqs. (11) and (12). This problem is a subject for a separate investigation.

As follows from the expression for u_m, the acoustic component of the soliton corresponds to compression deformation or tensile deformation if $(\partial\chi_m/\partial u)_0$ is positive or negative, respectively.

For possible experiments, the stability of soliton (13) under transverse perturbations is important. These perturbations are taken into account using Whitham's averaged Lagrangian method [15]. The system of Eqs. (11) and (12) corresponds to the Lagrangian density

$$L = \frac{i}{2}\left(\psi\frac{\partial\psi^*}{\partial z} - \psi^*\frac{\partial\psi}{\partial z}\right) + \frac{k_2}{2}\left|\frac{\partial\psi}{\partial\tau}\right|^2 + \alpha|\psi|^2\frac{\partial Q}{\partial\tau}$$
$$- \frac{c}{2n\omega_0}|\nabla_\perp\psi|^2 + \frac{\alpha}{2\beta}\left[\frac{\partial Q}{\partial\tau}\frac{\partial Q}{\partial z} - \frac{a}{2}(\nabla_\perp Q)^2\right], \tag{14}$$

where Q is related to the strain as $u = \partial Q/\partial\tau$.

Expressions (13) with the changes $1/\tau_p \longrightarrow \rho$, $qz \longrightarrow \Omega z/a - n\omega_0\Phi/c$ are used as trial solutions, where new dynamic variables ρ and Φ are coordinate functions that must be determined. Substituting trial solutions into Eq. (14) and integrating with respect to the fast variable τ (as was done in [16] for other nonlinear equations), we arrive at the average Lagrangian of the form

$$\Lambda \equiv \frac{c\alpha\beta}{2n\omega_0\Omega k_2^2}\int_{-\infty}^{+\infty} L d\tau = -\rho\frac{\partial\Phi}{\partial z} - \frac{1}{2}\rho(\nabla_\perp\Phi)^2$$
$$+ \frac{ck_2}{2n\omega_0}(\Omega^2\rho - \rho^3/3)$$
$$- \frac{c}{12n\omega_0}\left[\frac{c}{n\omega_0}\left(\frac{\pi^2}{6} + 2\right) + \frac{a}{2\Omega}\right]\frac{(\nabla_\perp\rho)^2}{\rho}. \tag{15}$$

Writing Euler–Lagrange equations for ρ and Φ with regard for Eq. (15), we obtain the "hydrodynamic-type" system

$$\frac{\partial\rho}{\partial z} + \nabla_\perp(\rho(\nabla_\perp\Phi)) = 0,$$
$$\frac{\partial\Phi}{\partial z} + \frac{(\nabla_\perp\Phi)^2}{2} + \frac{ck_2}{2n\omega_0}(\rho^2 - \Omega^2)$$
$$= \frac{c}{6n\omega_0}\left[\frac{c}{n\omega_0}\left(\frac{\pi^2}{6} + 2\right) + \frac{a}{2\Omega}\right]\left[\frac{\Delta_\perp\rho}{\rho} - \frac{(\nabla_\perp\rho)^2}{2\rho^2}\right]. \tag{16}$$

In the one-dimensional case, system (16) has the solutions $\rho = 1/\tau_p = \text{const}$ and $\Phi = \Phi_0(z) = (ck_2/2n\omega_0)(\Omega^2 - 1/\tau_p^2)z$, which exactly correspond to solitons (13). This circumstance is a serious argument in the favor of the average Lagrangian method.

The general analysis of Eq. (16) is complicated by its nonlinearity. For this reason, we take into account only small transverse perturbations corresponding to slight distortions of solitons (13). Accordingly, we write $\rho = 1/\tau_p + \rho_1$ and $\Phi = \Phi_0 + \Phi_1$, where $\rho_1 \ll 1/\tau_p$ and $\Phi_1 \ll \Phi_0$. Then, linearizing Eq. (16) with respect to ρ_1 and Φ_1 and setting $\rho_1, \Phi_1 \sim \exp[i(q_\parallel z + \mathbf{q}_\perp \mathbf{r}_\perp]$, we arrive at the "dispersion" relation

$$q_\parallel^2 = \frac{c}{2n\omega_0}\left\{\frac{k_2}{\tau_p^2} + \frac{1}{3}\left[\frac{c}{n\omega_0}\left(\frac{\pi^2}{6} + 2\right) + \frac{a}{2\Omega}\right]q_\perp^2\right\}q_\perp^2. \quad (17)$$

As was mentioned above, $k_2, \Omega > 0$. Therefore, the $q_\parallel$ values are real, and thereby the optical–acoustic soliton given by Eq. (13) is stable under small transverse perturbations.

Let us numerically estimate the parameters of the optical–acoustic soliton given by Eq. (13). The slowing of light in solids can be efficient when they are doped with rare-earth ions [2]. In [2], experiments on the slowing of light were carried out at a temperature of 5 K in the dielectric Y_2SiO_5 doped with 0.05 at. % of Pr ions. These ions were chosen because their quantum transitions in the above-indicated matrix are characterized by very narrow inhomogeneous broadening, and thereby the slowing of light can be most efficient. For the pumping intensity $I_p \approx 470$ W/cm^2, light in this medium has been slowed to $v_g \approx 4.5 \times 10^3$ cm/s. The speed of sound is approximately two orders of magnitude higher. The group velocity of the strongly slowed light component in the EIT regime is proportional to the Rabi frequency squared of the pumping field and, therefore, to intensity I_p [1]. Thus, in order to satisfy the condition $v_g \approx a$, I_p must be increased to 47 kW/cm^2. Let the soliton duration be $\tau_p \approx 100$ ps. In this case, for the parameters $\omega_0 \sim 10^{15}$ s^{-1}, $a \approx 5 \times 10^5$ cm/s, $\Omega \sim 10^{11}$ s^{-1}, $\rho_m \approx 2$ g/cm^3, $(\partial\chi_m/\partial u)_0 \sim \chi_m \sim 0.1$ [8], $n_m \sim 1$, and $k_2 \sim 1/a\omega_0$, we obtain $I_{\text{opt}} \approx c\psi_m^2/4\pi \sim 10^{-2}$ W/cm^2 for the intensity of the optical component of the soliton, $u_m \sim 10^{-9}$ for the strain, and $I_s \approx \rho_m a^3 u_m^2/2 \sim 10^{-8}$ W/cm^2 for the corresponding intensity of the acoustic component. Note that these estimates coincide in order of magnitude with the respective estimates presented in [4] for the nonsoliton regime of forward SMBS. Thus, for durations of several hundreds of picoseconds, the intensities of the optical–acoustic soliton are anomalously low, and the optical component dominates. As the duration of the soliton decreases, the intensity of the soliton, as well as the relative weight of the acoustic component, increases.

Anomalously low intensities of the optical component of the above soliton as compared to the intensities of the usual light solitons [9] are consistent with the conclusions made in [17, 18], where it was shown that the nonlinear characteristics of the medium in the EIT regime are giant and, correspondingly, are manifested for very low intensities of signal fields.

REFERENCES

1. L. V. Hau, S. E. Harris, Z. Dutton, and C. Behroozi, Nature **397**, 594 (1999).
2. A. V. Turukhin, V. S. Sudarshanam, M. S. Shahriar, *et al.*, Phys. Rev. Lett. **88**, 023602 (2002).
3. A. B. Matsko, Yu. V. Rostovtsev, H. Z. Cummins, and M. O. Scully, Phys. Rev. Lett. **84**, 5752 (2000).
4. A. B. Matsko, Yu. V. Rostovtsev, M. Fleishhauer, and M. O. Scully, Phys. Rev. Lett. **86**, 2006 (2001).
5. A. V. Gulakov and S. V. Sazonov, Pis'ma Zh. Éksp. Teor. Fiz. **79**, 746 (2004) [JETP Lett. **79**, 610 (2004)].
6. A. A. Zabolotskiĭ, Zh. Éksp. Teor. Fiz. **126**, 155 (2004) [JETP **99**, 133 (2004)].
7. S. V. Sazonov, Pis'ma Zh. Éksp. Teor. Fiz. **76**, 176 (2002) [JETP Lett. **76**, 143 (2002)].
8. R. H. Pantell and H. E. Puthoff, *Fundamentals of Quantum Electronics* (Wiley, New York, 1969; Mir, Moscow, 1972).
9. S. A. Akhmanov, V. A. Vysloukh, and A. S. Chirkin, *The Optics of Femtosecond Laser Pulses* (Nauka, Moscow, 1988) [in Russian].
10. S. E. Harris, Phys. Today, No. 7, 36 (1997).
11. S. E. Harris, J. E. Field, and A. Kasapi, Phys. Rev. A **46**, R29 (1992).
12. V. E. Zakharov, Zh. Éksp. Teor. Fiz. **62**, 1745 (1972) [Sov. Phys. JETP **35**, 908 (1972)].
13. R. K. Dodd, J. C. Eilbeck, J. D. Gibbon, and H. C. Morris, *Solitons and Nonlinear Wave Equations* (Academic, London, 1984; Mir, Moscow, 1988).
14. N. Yadjima and M. Oikawa, Prog. Theor. Phys. **56**, 1719 (1976).
15. S. K. Zhdanov and B. A. Trubnikov, Zh. Éksp. Teor. Fiz. **92**, 1612 (1987) [Sov. Phys. JETP **65**, 904 (1987)].
16. S. V. Sazonov, Zh. Éksp. Teor. Fiz. **125**, 1409 (2004) [JETP **98**, 1237 (2004)].
17. H. Schmidt and A. Imamoglu, Opt. Lett. **21**, 1936 (1996).
18. M. Lukin and A. Imamoglu, Phys. Rev. Lett. **84**, 1419 (2000).

Translated by R. Tyapaev

JETP Letters, Vol. 81, No. 5, 2005, pp. 205–208. Translated from Pis'ma v Zhurnal Éksperimental'noĭ i Teoreticheskoĭ Fiziki, Vol. 81, No. 5, 2005, pp. 263–267.

Dynamic Effect of Collision Phase Lockout in a Gas of Cold "Dark" Atoms

L. V. Il'ichev

Institute of Automatics and Electrometry, Siberian Division, Russian Academy of Sciences, Universitetskiĭ pr. 1, Novosibirsk, 630090 Russia

e-mail: leonid@iae.nsk.su

Received December 16, 2004; in final form, January 14, 2005

In a gas of slow atoms exhibiting the effect of coherent population trapping (CPT) on the sublevels of the ground state in a spatially nonuniform light field, rare collisions destroying the CPT state initiate the irreversible exchange of momentum between radiation and atoms. This exchange is manifested as an additional force that acts on the particles and is of geometric origin; i.e., it is determined only by the structure of the field of local CPT states. When this force is not masked by the standard collision change in atomic momentum, the observation of the kinetics of the particles may provide information on the physics of the collisions. © *2005 Pleiades Publishing, Inc.*

PACS numbers: 32.80.Qk, 42.50.–p

The evolution of an atom that interacts with resonant radiation and has a complicated structure of the sublevels of its ground state exhibits the phenomenon of coherent population trapping (CPT). This phenomenon includes numerous effects known from the early development stages of the physics of the interaction between resonant radiation and gaseous media. Investigations of optical pumping (see review [1]) were the first in this series. The development of the test-field method in nonlinear laser spectroscopy of three-level systems also led to the observation of the effect now known as CPT [2]. A wide interest in the CPT phenomenon was initiated by [3]. It is now applied in such important fields as superhigh-resolution spectroscopy (so-called "dark resonance") [4], nonlinear optics [5], creation of an inversionless laser [6], atomic optics [7], and laser cooling of atoms below the photon recoil energy [8]. States of CPT may also be used as a fine instrument for studying interparticle interactions in a rarefied gas. As is known, these states are certain superpositions of the atomic states on certain atomic sublevels. Controlling the amplitudes of these states by varying the parameters of the radiation field, one may observe the kinetics of atoms and thereby analyze the dependence of the result of a collision on the internal state of the particles. A simple example of such an approach is the subject of this work.

We remind readers of the essence of the CPT phenomenon, which is observed even in the simplest standard model of a Λ atom interacting with a pair of monochromatic light fields (see figure). This scheme, along with the notation introduced in it, will be used below. A certain uncoupled superposition $|\psi^{UNC}\rangle$ of the ground states $|-\rangle$ and $|+\rangle$ turns out to be "dark"; i.e., it is not involved in the radiative evolution of the atom. The processes of induced radiative transitions $|\psi^{UNC}\rangle \longrightarrow |0\rangle$ through the channels $|-\rangle \longrightarrow |0\rangle$ and $|+\rangle \longrightarrow |0\rangle$ destructively interfere and damp each other, because the amplitudes of states $|-\rangle$ and $|+\rangle$ in the superposition $|\psi^{UNC}\rangle$ are matched with the amplitudes λ_- and λ_+ of the optical transition per unit time (the explicit form of the state $|\psi^{UNC}\rangle$ will be introduced below). The inclusion of the spatial dependence of the optical transition amplitudes $\lambda_\pm = \lambda_\pm(x)$ leads to the notion of the local CPT state $|\psi^{UNC}(x)\rangle$. The atom reaches the dark state due to a series of induced and spontaneous radiative transitions. In this work, the fast (primarily compared to translational motion) transition of the atom to the CPT state is analyzed. Under these conditions, the introduction of the notion of the local CPT state is reasonable.

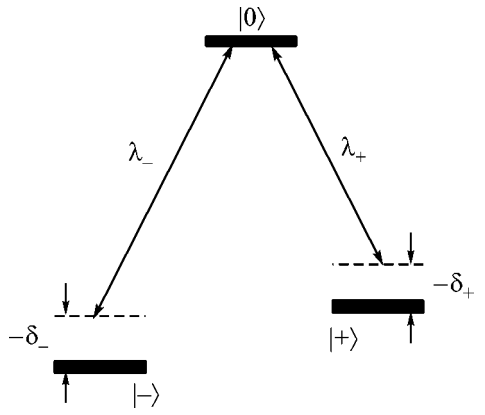

Scheme of the Λ-atom levels.

The slow atom reaching the dark state does not leave it. This model was first considered in [9], where the conditions of its applicability were derived.

Let us assume that a movable dark atom collides with buffer gas particles. We ignore the interparticle momentum exchange and suppose that random change (lockout) in the relative phase of the states $|-\rangle$ and $|+\rangle$ is the only collision effect. Thus, after a collision, the atom is in a state from which optical transitions are possible. In the process of fast radiative evolution, the atom is an intermediary in the exchange of photons between different plane waves of the laser radiation field and the field of spontaneous photons. After this evolution, the atom that is not displaced again reaches the dark state, gaining a certain momentum. Thus, the process of the destruction of the CPT state in collision phase lockout initiates the transfer of the momentum from radiation to the atom. A certain additional force begins to act on the atom. This work is devoted to the calculation of this force in the above-indicated approximations.

We start with the following quantum kinetic equation for the atomic density matrix $\hat{\varrho}$:

$$\partial_t\hat{\varrho} + \frac{i}{2m}[\hat{p}^2, \hat{\varrho}] = \mathcal{R}[\hat{\varrho}] + \mathcal{C}[\hat{\varrho}]. \quad (1)$$

The left-hand side of this equation includes the Hamiltonian of translational motion ($\hat{p}$ and m are the momentum operator and mass of the atom, respectively). The first term on the right-hand side is the Liouvillian of the proper internal dynamics of the atom and its interaction with radiation through induced and spontaneous transitions. In the coordinate representation, it is appropriate to introduce a superoperator $\mathcal{R}(x_1, x_2)$ that acts on the internal degrees of freedom of the atom and depends parametrically on x_1 and x_2:

$$\begin{aligned}\langle x_1|\mathcal{R}[\hat{\varrho}]|x_2\rangle &\equiv \mathcal{R}(x_1, x_2)[\hat{\varrho}(x_1|x_2)]\\ &= -i\delta_+[\hat{P}_+, \hat{\varrho}(x_1|x_2)] - i\delta_-[\hat{P}_-, \hat{\varrho}(x_1|x_2)]\\ &- i\hat{V}(x_1)\hat{\varrho}(x_1|x_2) + i\hat{\varrho}(x_1|x_2)\hat{V}(x_2)\\ &+ (\Gamma_+(x_1 - x_2)\hat{P}_+ + \Gamma_-(x_1 - x_2)\hat{P}_-)\mathrm{Tr}\hat{P}_0\hat{\varrho}(x_1|x_2)\\ &- \frac{1}{2}(\gamma_+ + \gamma_-)(\hat{P}_0\hat{\varrho}(x_1|x_2) + \hat{\varrho}(x_1|x_2)\hat{P}_0).\end{aligned} \quad (2)$$

Here, $\delta_\pm$ is the detuning from the resonant frequencies corresponding to the transition $|\pm\rangle \longrightarrow |0\rangle$, $\hat{P}_\alpha$ are the projectors on the corresponding states,

$$\hat{V}(x) = \lambda_+(x)|0\rangle\langle+| + \lambda_-(x)|0\rangle\langle-| + \text{h.c.}$$

is the Hamiltonian of interaction with the field, and $\gamma_\pm$ are the rates of spontaneous decays through the corresponding channels. The coordinate dependence of rates $\Gamma_\pm$ in the income terms is associated with the inclusion of the recoil momentum in the emission of a spontaneous photon (see, e.g., [10]). The particular form of these functions is immaterial in this work. It is sufficient to remember that $\Gamma_\pm(x) = \Gamma_\pm(|x|)$ and $\Gamma_\pm(x) \longrightarrow \gamma_\pm$ for $x \longrightarrow 0$. In superoperator (2), as well as in initial equation (1), a unitary transformation was performed that removed an explicit harmonic time dependence of the Hamiltonian $\hat{V}(x)$. Possible fluctuations of fields $\lambda_\pm(x)$ are disregarded.

The second term on the right-hand side of Eq. (1) describes the collision destruction of the coherent superpositions of states $|+\rangle$ and $|-\rangle$:

$$\mathcal{C}[\hat{\varrho}] = \nu(\hat{P}_+\hat{\varrho}\hat{P}_+ + \hat{P}_-\hat{\varrho}\hat{P}_- - \hat{\varrho}), \quad (3)$$

where ν is the collision frequency.

In what follows, the dark-resonance condition $\delta_+ = \delta_- \equiv \delta$ is assumed to be satisfied. Under this condition, the state

$$|\psi^{\mathrm{UNC}}(x)\rangle = \frac{\lambda_-(x)}{\lambda(x)}|+\rangle - \frac{\lambda_+(x)}{\lambda(x)}|-\rangle \quad (4)$$

(where $\lambda^2(x) \equiv |\lambda_+(x)|^2 + |\lambda_-(x)|^2$) is not involved in interaction with the field; i.e.,

$$\mathcal{R}(x_1, x_2)[|\psi^{\mathrm{UNC}}(x_1)\rangle\langle\psi^{\mathrm{UNC}}(x_2)|] = 0. \quad (5)$$

As was mentioned above, the evolution of the atom to the dark state is assumed to be fast in our model; i.e., the atom is not displaced and does not undergo collisions. Under this condition, the equation

$$\partial_t\hat{\varrho} = \mathcal{R}[\hat{\varrho}] \quad (6)$$

describes this evolution with a high accuracy. The result of this evolution may be symbolically represented as the result of the action of a certain superoperator $\mathcal{D}$:

$$\hat{\varrho}^{(\mathrm{post})} = \mathcal{D}[\hat{\varrho}^{(\mathrm{pre})}]. \quad (7)$$

As in $\mathcal{R}$, in the coordinate representation it is convenient to introduce the superoperator $\mathcal{D}(x_1, x_2)$ that depends parametrically on x_1 and x_2 and acts only in the space of the internal atomic states:

$$\langle x_1|\mathcal{D}[\hat{\varrho}^{(\mathrm{pre})}]|x_2\rangle = \mathcal{D}(x_1, x_2)[\hat{\varrho}^{(\mathrm{pre})}(x_1|x_2)]. \quad (8)$$

The result of the application of the superoperator $\mathcal{D}(x_1, x_2)$ always has the form

$$\hat{\varrho}^{(\mathrm{post})}(x_1|x_2) = |\psi^{\mathrm{UNC}}(x_1)\rangle\varrho(x_1|x_2)\langle\psi^{\mathrm{UNC}}(x_2)|, \quad (9)$$

where all the information on $\hat{\varrho}^{(\mathrm{pre})}(x_1|x_2)$ is contained in the function $\varrho(x_1|x_2)$.

As a result, evolution for time scales longer than the duration of evolution to the dark state is described by the kinetic equation

$$\partial_t \hat{\varrho} + i[\hat{K}(\hat{x}), \hat{\varrho}] = \nu \sum_{\sigma = \pm} \mathcal{D}[\hat{P}_\sigma \hat{\varrho} \hat{P}_\sigma] - \nu \hat{\varrho}. \quad (10)$$

The density matrix entering into this equation satisfies, according to Eq. (9), the condition $\hat{\varrho} = \hat{P}^{\mathrm{UNC}}(\hat{x})\hat{\varrho} = \hat{\varrho}\hat{P}^{\mathrm{UNC}}(\hat{x})$, where $\hat{P}^{\mathrm{UNC}}(\hat{x})$ is the projection operator on the local CPT state. The contribution of the translational motion is presented in the operator $\hat{K}(\hat{x}) = \hat{P}^{\mathrm{UNC}}(\hat{x})\hat{p}^2/2m\hat{P}^{\mathrm{UNC}}(\hat{x})$. Such a modification of the initial Hamiltonian corresponds to the adiabaticity model used here for the transitional motion and presents, as is easily verified, the dynamics of the atom in the field of the scalar and vector potentials of the geometric origin [9, 11, 12]. We are interested in the right-hand side of Eq. (10), which presents the collision destruction of the CPT state and, as a result, the irreversible transfer of the momentum of the atom to the radiation field. In order to calculate collision effects, it is necessary to know the action $\mathcal{D}(x_1, x_2)$ in explicit form, i.e., to express $\varrho(x_1|x_2)$ from Eq. (9) in terms of $\hat{\varrho}^{(\mathrm{pre})}(x_1|x_2)$. To this end, we use the following approach [9]. Note that the Hilbert–Schmidt scalar product

$$((\hat{\rho}, \hat{\varrho})) \equiv \mathrm{Tr}\hat{\rho}^\dagger \hat{\varrho} \quad (11)$$

is an integral of Eq. (6) if the operator $\hat{\rho}$ is canceled by the action of the superoperator $\mathcal{R}^\dagger$ conjugate to the superoperator $\mathcal{R}$ with respect to scalar product (11). In this case, it is easy to see that

$$((\hat{\rho}, \hat{\varrho}^{(\mathrm{post})})) = ((\hat{\rho}, \mathcal{D}[\hat{\varrho}^{(\mathrm{pre})}])) = ((\hat{\rho}, \hat{\varrho}^{(\mathrm{pre})})). \quad (12)$$

The operator $\hat{\varrho}^{(\mathrm{post})}(x_1|x_2)$ is uniquely determined from the above equality. Trivial algebra shows that $\hat{\rho}(x_1, x_2)$: $\mathcal{R}^\dagger(x_1, x_2)[\hat{\rho}(x_1, x_2)] = 0$.

The result of the calculation of the right-hand side of Eq. (10) in the coordinate representation has the form

$$\nu(f(x_1, x_2) - 1)\hat{\varrho}(x_1|x_2), \quad (13)$$

where

$$f(x_1, x_2) = \frac{A(x_1, x_2)}{B(x_1, x_2)}. \quad (14)$$

Here,

$$\begin{aligned} A(x_1, x_2) &= 2\gamma(\lambda_+(x_1)\lambda_+^*(x_2)\Gamma_+(x_1 - x_2) \\ &\quad - \lambda_-(x_1)\lambda_-^*(x_2)\Gamma_-(x_1 - x_2)) \\ &\times (|\lambda_+(x_1)|^2\lambda^2(x_2) - \lambda^2(x_1)|\lambda_-(x_2)|^2) \\ &\quad - (|\lambda_+(x_1)\lambda_+(x_2)|^2 + |\lambda_-(x_1)\lambda_-(x_2)|^2) \\ &\times [2i\gamma\delta(\lambda^2(x_1) - \lambda^2(x_2)) + (\lambda^2(x_1) - \lambda^2(x_2))^2 \\ &\quad + 2\gamma^2(\lambda^2(x_1) + \lambda^2(x_2))]; \end{aligned} \quad (15)$$

$$\begin{aligned} B(x_1, x_2) &= \lambda^2(x_1)\lambda^2(x_2) \\ &\times [2\gamma(\lambda_+(x_1)\lambda_+^*(x_2)\Gamma_+(x_1 - x_2) \\ &\quad + \lambda_-(x_1)\lambda_-^*(x_2)\Gamma_-(x_1 - x_2)) \\ &\quad + 2i\gamma\delta(\lambda^2(x_1) - \lambda^2(x_2)) - (\lambda^2(x_1) - \lambda^2(x_2))^2 \\ &\quad - 2\gamma^2(\lambda^2(x_1) + \lambda^2(x_2))], \end{aligned} \quad (16)$$

where $\gamma \equiv (\gamma_+ + \gamma_-)/2$. The function $f(x_1, x_2)$ ($f^*(x_1, x_2) = f(x_2, x_1)$) represents the change in the transitional motion state when the atom gains momentum from the radiation field. Note that $f(x_1, x_2) \longrightarrow 1$ for $x_1 \longrightarrow x_2$.

A force appears in the explicit form in the Wigner representation for the description of the motion of the atom (see, e.g., [10]). Under the assumption that the coherence length of the atomic wave packet is shorter than the characteristic scales (e.g., wavelength) at which the amplitudes $\lambda_\pm(x)$ vary, expression (13) assumes the standard classical kinetic form

$$-F(x)\partial_p \hat{\varrho}(x, p), \quad (17)$$

where

$$F(x) = i\frac{\nu}{2}\partial_{x'}[f(x, x') - f(x', x)]\Big|_{x' = x}. \quad (18)$$

The final expression for the force has the form

$$\begin{aligned} F(x) &= -i\nu\frac{\gamma_+|\lambda_-(x)|^2[\lambda_+^*(x)\overleftrightarrow{\partial}_x\lambda_+(x)]}{\lambda^2(x)(\gamma_+|\lambda_-(x)|^2 + \gamma_-|\lambda_+(x)|^2)} \\ &\quad - i\nu\frac{\gamma_-|\lambda_+(x)|^2[\lambda_-^*(x)\overleftrightarrow{\partial}_x\lambda_-(x)]}{\lambda^2(x)(\gamma_+|\lambda_-(x)|^2 + \gamma_-|\lambda_+(x)|^2)} \\ &\quad + 2\delta\nu\frac{|\lambda_+(x)|^4 + |\lambda_+(x)\lambda_-(x)|^2 + |\lambda_-(x)|^4}{\lambda^4(x)(\gamma_+|\lambda_+(x)|^2 + \gamma_-|\lambda_-(x)|^2)}\partial_x\lambda^2(x), \end{aligned} \quad (19)$$

where the standard notation $a\overleftrightarrow{\partial}_x b = a\partial_x b - b\partial_x a$ is used. For traveling light waves ($\lambda_\pm(x) = \lambda_\pm \exp(ik_\pm x)$), the first two terms on the right-hand side of Eq. (19) are nonzero. The force in the case of standing waves is given by the last term. In this case, this force turns out to be an antisymmetric function of frequency detuning δ. Note that the force $F(x)$ is independent of the radiation intensity; more precisely, it is invariant under the transformation $\lambda_\pm(x) \longrightarrow \mathrm{const}\lambda_\pm(x)$. This property is attributed to the fact that only the structure of the field of the

CPT states $|\psi^{UNC}(x)\rangle$ is important for determining the force, because the transition to the dark state is the fastest process. Owing to this circumstance, force (19) is similar to the aforementioned geometric potentials.

The first two terms in Eq. (19) are of the order of νk, where k is the characteristic wave vector of the radiation field. The variation of the relative values of the parameters $\lambda_\pm$ and $\gamma_\pm$ changes this estimate only slightly. The third term contains the detuning δ. If the detuning is too large, the time of the arrival of the atom at the dark state is comparable with the time of flight k^{-1} of the characteristic scale of inhomogeneity and our model becomes incorrect. Using these criteria, we estimate the upper allowable limit for $|\delta|$ under the assumption that $kv \ll \gamma, \lambda$ (v is the characteristic atomic velocity, and $\gamma \simeq \gamma_\pm$). For $|\delta| \ll \gamma$ and λ, the condition of the slowness of the atomic motion compared to the occupation rate of the dark state has the form [9] $kv \ll \gamma\lambda^2/\delta^2$. Therefore, $|\delta| \ll \lambda\sqrt{\gamma/kv}$. The right-hand side of this inequality is the desired limit. The third term in the expression for the force at limiting detuning is estimated as $\sim\nu\lambda\sqrt{k/\gamma v}$. For $\lambda \sim \gamma \sim 10^8$ s^{-1} and $kv \sim 10^6$ s^{-1}, this estimate is an order of magnitude larger than νk. For a dipole moment of about $15D$ (as for rubidium), the necessary intensity is equal to 20 mW/cm^2.

Thus, we have considered the kinetic manifestation of specific "quasi-optical" collisions that are combined events consisting of a usual collision and the following short (about the characteristic time of system evolution) stage of the interaction of the atom with the radiation field. The situation of the collision lockout of the relative phase in the superposition of vectors $|+\rangle$ and $|-\rangle$ has been analyzed. This basis is separated in the subspace of the ground atomic states in its proper internal dynamics of the atom (by assumption, it diagonalizes the proper internal Hamiltonian) and in its interaction with radiation. Note that the introduced spontaneous decay rates γ_+ and γ_- are also connected with this basis. When the energies of the sublevels of the ground state are equal to each other (these energies are different in figure), the collision destruction of coherence between states from a certain "rotated" basis $|1\rangle = \alpha|+\rangle + \beta|-\rangle$ and $|2\rangle = -\beta^*|+\rangle + \alpha^*|-\rangle$, where $|\alpha|^2 + |\beta|^2 = 1$, is possible.[1] In this case, Eq. (3) contains the projection operators $\hat{P}_1$ and $\hat{P}_2$ on the turned state rather than $\hat{P}_+$ and $\hat{P}_-$. The dynamics of coherence with respect to the old basis turns out to be more complicated, and collision transitions $|+\rangle \longleftrightarrow |-\rangle$ appear. Expression (19) for the force is significantly modified. This property illustrates the statement made at the beginning of the paper that CPT states are applicable to investigation of collisions. The rigorous model must evidently take into account both change in the atomic momentum during collision and the real, more complicated structure of the sublevels of the ground state. In such a model, as well as in experiments, the problem of the detection of force (19) against the background of collision change in the moment will arise.

[1] If the energies of the states $|+\rangle$ and $|-\rangle$ are different, the collision superoperator describing the destruction of coherence in the superposition of $|1\rangle$ and $|2\rangle$ is not invariant under the unitary transformation of the "rotating wave" that is performed in Eq. (1).

I am grateful to A.V. Taĭchenachev, P.L. Chapovskiĭ, and A.M. Shalagin for detailed discussion of the problems analyzed in this work. This work was supported by the Russian Foundation for Basic Research (project nos. 03-02-17553 and 04-02-16771) and the Siberian Division of the Russian Academy of Sciences (integration project "Cooling of Gases in Magneto-Optical Traps").

REFERENCES

1. W. Happer, Rev. Mod. Phys. **44**, 169 (1972).
2. T. Ya. Popova, A. K. Popov, S. G. Rautian, and R. I. Sokolovskiĭ, Zh. Éksp. Teor. Fiz. **57**, 850 (1969) [Sov. Phys. JETP **30**, 466 (1970)].
3. G. Alzetta, A. Gozzini, L. Moi, and G. Orriols, Nuovo Cimento **36**, 5 (1976).
4. A. Akulshin, A. Celikov, and V. Velichansky, Opt. Commun. **84**, 139 (1991).
5. J. E. Field, K. H. Hahn, and S. E. Harris, Phys. Rev. Lett. **67**, 3062 (1991).
6. M. O. Scully, Phys. Rep. **129**, 191 (1992).
7. P. Marte, P. Zoller, and J. L. Hall, Phys. Rev. A **44**, 4118 (1991).
8. A. Aspect, E. Arimondo, R. Kaiser, *et al.*, Phys. Rev. Lett. **61**, 826 (1988).
9. A. V. Taichenachev, A. M. Tumaikin, and V. I. Yudin, Laser Phys. **2**, 575 (1992).
10. S. G. Rautian and A. M. Shalagin, *Kinetic Problems of Nonlinear Spectroscopy* (Elsevier, Amsterdam, 1991).
11. R. Dum and M. Olshanii, Phys. Rev. Lett. **76**, 1788 (1996).
12. P. M. Visser and G. Nienhuis, Phys. Rev. A **57**, 4581 (1998).

Translated by R. Tyapaev

JETP Letters, Vol. 81, No. 5, 2005, pp. 209–213. Translated from Pis'ma v Zhurnal Éksperimental'noĭ i Teoreticheskoĭ Fiziki, Vol. 81, No. 5, 2005, pp. 268–273.

Motion of an Atom under the Effect of Femtosecond Laser Pulses: From Chaos to Spatial Localization

V. I. Balykin

Institute of Spectroscopy, Russian Academy of Sciences, Troitsk, Moscow region, 142190 Russia
Institute for Laser Science, University of Electrocommunications, Chofugaoka, Chofushi, Tokyo 182, Japan

Received January 20, 2005

The spatial localization of an atom in a field of periodic femtosecond laser pulses is considered. It has been shown that the atom can be localized with absolute accuracy in the nanometer range. The time interval during which the atom is situated in the laser field is only 10^{-7}–10^{-8} of the total localization time interval. © *2005 Pleiades Publishing, Inc.*

PACS numbers: 32.80.Pj

A single atom "at rest" is an ideal physical object for many fundamental and applied investigations [1–3]. A good approximation is an atom that is cooled by laser light and localized in one of the diversiform traps that have been realized to date [4–6]. However, a potential localizing the atom provides an appreciable perturbing effect on both external and internal degrees of freedom of the atom (shift of the atomic energy levels, modulation of the position and velocity of the atom, etc.). The best situation that may be expected (which has been achieved in certain types of traps) is the cooling of the atom to a temperature corresponding to the energy of the atomic ground state, where the atom occupies the minimum phase space. Although the spatial motion of the atom is minimal in the ground state, this motion noticeably affects the internal degrees of freedom (shift of energy levels, etc.). Most fundamental and applied investigations are focused on the internal degrees of freedom. In the method that was proposed by Karori *et al.* [7] (and was realized in the experiment reported in [8]) for minimizing the effect of the localizing potential on certain internal degrees of freedom of the atom, the atom-localization conditions under which the effect of the spatial motion of the atom on its internal degrees of freedom is minimal are realized by varying the parameters of the trap. In the experiment reported in [8], the minimum effect on the shift of the atomic absorption line (transition between two energy levels) was realized by choosing the parameters of the trap for which the shifts of both levels were very close to each other. As a result, the effect of the potential on the atomic parameter of interest is minimized.

Traps are intended for trapping various particles in a limited spatial region. This aim is achieved by imposing a certain potential, which is usually time-independent, on this region. The time-independent potential is used because particles usually have high velocities. In particular, an atom with a thermal velocity of about 10^5 cm/s is displaced in space by 1 mm for only 1 μs. Significant advances in the field of the laser cooling of atoms has provided the possibility of dealing with velocities of about equal to or even lower than the recoil velocities $v_r \sim 1$ cm/s. For such low velocities, the concept of using time-independent confining potentials becomes unnecessary.

In this work, we propose and analyze another approach to the minimization of the effect of the localizing field on the atom. Its essence is the use of the *short-term and time-periodic* action of the laser field on the spatial motion of a *very slow* atom. In such a scheme, the atom is free of the perturbing effect (for the use of the atom for measurements) of the localizing field for a certain time interval $(1 - t_p/T)$, where t_p is the duration of the action and T is its repetition period. When femtosecond pulses are used, the relative time interval during which the atom is situated in the localizing field may be very short, i.e., 10^{-7}–10^{-6} of the total time interval during which the atom is confined in the trap. As will be shown below, the approach under consideration may provide the situation wherein the atom is subjected to the localizing field for only $(10^{-8}$–$10^{-9})$% of the total time interval of its localization; i.e., the atom is *almost at rest.*

The behavior of the particle under the action of periodic short force pulses has been actively studied in connection with the problem of classical and quantum chaos [9, 10]. We will show that, under certain (experimentally realizable) conditions, it is possible to avoid chaos in the motion of the atom and to achieve its long-term spatial localization.

The basic idea of the localization of the atom by a periodic sequence of short laser pulses is as follows. Laser light pulses are perpendicularly reflected from a mirror. The incident and reflected pulses "collide" at a certain distance from the mirror. The energy of a single

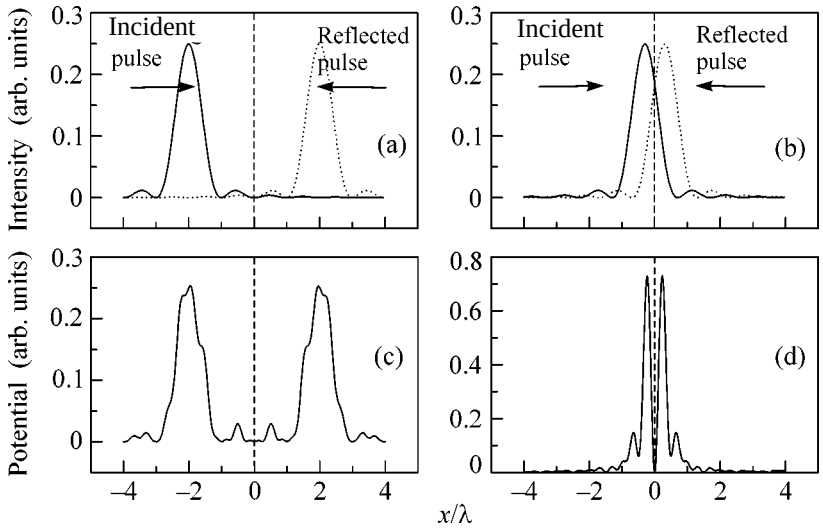

Fig. 1. (c, d) Shapes of the atomic potential for two relative positions (a, b) of two counter-propagating (incident and reflected) femtosecond laser pulses.

femtosecond pulse is spatially localized at a size $l = c/t_p$, where c is the speed of light and t_p is the pulse duration. When the duration of the laser pulse is extremely short, i.e., equal to the period of light [11], its spatial size is equal to the laser wavelength: $l = \lambda$. The region where pulses collide is the localization region for the atom and has the same size. Depending on the phase relations between the incident and reflected pulses, either a maximum or minimum of the laser-field intensity arises at the center of the overlapping of the pulses due to their interference. The atom that is placed in the pulse collision region is subjected to the gradient force of light pressure that is directed toward the center of the pulse overlapping region when the laser frequency is lower than the atomic transition frequency and intensity is maximal. (When femtosecond few-cycle light pulses are used, several minima of the potential energy arise.) After the action of a light pulse, the atom freely moves with a velocity determined by its initial velocity and the momentum gained from the laser field. Figures 1c and 1d show the shapes of the localizing potential for two different positions of two laser pulses shown in Figs. 1a and 1b, respectively.

The basic questions that concern the above procedure and answers to which are sought in this work are as follows. The first is whether the motion of atoms is finite in the coordinate and momentum spaces. The second is whether the action of short intense laser pulses is breaking for atom (i.e., whether the atom is ionized or dynamic chaos arises).

Let us consider a two-level atom that is characterized by an absorption frequency of ω_0 and interacts with a quasi-resonant laser field with a frequency ω_L. When the detuning $\delta = \omega_0 - \omega_L$ is sufficiently large, the upper-level population may be disregarded (adiabatic elimination). In this case, the atom may be treated as a structureless pointlike particle. For the field intensity that is required for the localization of the atom (see below), the two-level approximation is valid for the interaction of the atom with the strong field [12]. In these approximations and in the one-dimensional case, the Hamiltonian of the interaction of the atom with a sequence of laser pulses has the form [13]

$$H = H_0 + V(t)\sum_n F(t - nT). \quad (1)$$

Here, $H_0 = P^2/2M$, where P is the momentum of the atom; $V(t) = V_0\cos(2k_L X)$; and $F(t)$ describes the time profile of the laser field consisting of pulses that have duration t_p and follow with period T. The potential has a period of half the wavelength, and its amplitude is given by the expression

$$V_0 = \hbar\Omega_R^2/8\delta. \quad (2)$$

Here, $\Omega_R = 2\mu E_0/\hbar$ is the Rabi frequency, where μ is the matrix element of the atomic dipole moment and E_0 is the amplitude of the electric field of the laser wave. It is convenient to represent Hamiltonian (1) in the dimensionless form

$$H' = H_0' + V'(t)\sum_n f(\tau - n). \quad (3)$$

Here, $H_0' = \rho^2/2$, where $\rho = (2k_L T/M)P$ is the dimensionless momentum; $V'(t) = k\cos x$, where $x = 2k_L X$ is the dimensionless coordinate, $k_L = 2\pi/\lambda$, λ is the laser wavelength, $k = (8V_0/\hbar)\omega_r T^2$ is the normalized potential amplitude, $\omega_r = \hbar k_L^2/2M$ is the recoil frequency, and M is the atomic mass; $\tau = t/T$ is the dimensionless time; and the function $f(\tau)$ describes the time dependence of the laser field (with the unit amplitude of a laser pulse

of duration t_p/T). In the limit of infinitely short pulses, when $f(\tau)$ is the Dirac delta function, Hamiltonian (3) has the form

$$H' = \rho^2/2 + K\cos\phi\sum_n \delta(\tau - n), \quad (4)$$

where $K = \beta k$ is the stochasticity parameter and $\beta = \int F(t)dt/t_p$ is the factor that depends on the laser field shape and is close to unity. Hamiltonian (4) also describes the dynamics of a δ-kicked rotator, which has been actively studied in the problem of classical and quantum chaos [9, 10].

First, let us estimate the orders of magnitude of the parameters of laser pulses and atoms for which atoms may be spatially localized. We analyze the case of extremely short laser pulses whose duration is equal to the light-wave period $t_p = 2\pi/\omega$. This case is of most interest, because atoms may be localized with absolute accuracy in the nanometer range. We also suppose that the spectral width $\Delta\omega_L$ of the laser pulse is significantly narrower than the detuning between the central radiation frequency and the atomic transition frequency; i.e., $\Delta\omega_L < \delta$. If the initial atomic velocity is such that, for a time interval between pulses, the atom is displaced insignificantly compared to the characteristic size of the pulse-overlapping region (atom localization region), then, under the above conditions, one can say that the atom is subjected to the average potential with the amplitude

$$\tilde{V}(x) = V(x)\frac{t_p}{T} = \frac{\hbar\Omega_R^2(x)}{8\delta}\frac{t_p}{T}. \quad (5)$$

A necessary condition for the localization of the atom in such a potential is that the potential barrier must be higher than the kinetic energy of the atom. This condition leads to the following relation between the initial atomic velocity v_{at} and the parameters of laser pulses:

$$v_{at} \le \alpha^2 v_r\left(\frac{t_p}{T}\frac{1}{\omega_r\delta}\right)^{1/2}\Omega_R = \alpha^2\gamma v_r\left(\frac{t_p}{2T}\frac{1}{\omega_r\delta}\frac{I}{I_S}\right)^{1/2}. \quad (6)$$

Here, $\alpha \equiv v_{at}/v_r$, v_r is the recoil velocity, 2γ is the width of the upper atomic level, I_S is the intensity of the saturation of the atomic transition, and I is the time-averaged intensity of the laser field in the overlapping region for laser pulses. The localization of the atom is achieved for the following average intensity of laser radiation:

$$I = \alpha^2\frac{\omega_r\delta}{2\gamma^2}I_S. \quad (7)$$

The peak intensity of the laser field is

$$I_p = \alpha^2\frac{\omega_r\delta}{2\gamma^2}\frac{T}{t_p}I_S, \quad (8)$$

and the peak Rabi frequency is given by

$$\Omega_R = \frac{\alpha}{2}\left(\omega_r\delta\frac{T}{t_p}\right)^{1/2}. \quad (9)$$

For example, for the Rb atom and laser radiation with a central frequency of 1.06 μm (Nd^{3+}:YAG laser), these parameters are $I = \alpha^2 50$ W/cm^2, $I_p = \alpha^2 1.2\times10^8$ W/cm^2, and $\Omega_R = 2\pi\alpha 5\times10^{11}$ s^{-1}. If laser radiation is focused to a size of $d = 30$ μm, the required average power of laser radiation is as small as $P = \alpha^2 0.5$ mW. An important consequence of the above estimate is that, for atomic velocities lower than the recoil velocity ($\alpha < 1$), the peak intensity that is required for the localization of the atom is several orders of magnitude lower than values for which the ionization of the atom occurs in the field of femtosecond pulses [14].

Note that few-cycle pulsed laser systems with the above-presented energy parameters really exist in laboratories [11].

The lifetime of the atom in optical dipole traps is fundamentally limited by the velocity diffusion of the atom due to spontaneously emitted photons of the localizing laser field. The so-called hyperbolic secant is quite a close approximation for the shape of a separate femtosecond laser pulse. In this approximation, the probability of the excitation of the atom to the upper level by an individual pulse is given by the expression [15]

$$W(t \gg t_p) = \exp(-t/t_{sp})\sin^2(\Omega_R t_p)\left[\operatorname{sech}\frac{1}{2}(\delta t_p + \gamma t_p/2)\right]^2, \quad (10)$$

where t_{sp} is the radiative lifetime of the given atomic transition. When the laser pulse duration is much shorter than the lifetime of the excited state ($t_p \ll 1/2\gamma$), the probability of the excitation of the atom is related to the parameters of the atom and laser pulse as follows:

$$W(t \gg t_p) = \alpha^2\frac{\omega_r\delta T t_p}{\exp(\delta t_p)}. \quad (11)$$

For the case where the pulse period is longer than the relaxation time for the excited state ($T \gg 1/2\gamma$) (disregarding the quantum interference effect in the excitation of the atom) and the "area" of the pulse satisfies the relation $\Omega_R t_p \ll 1$, it follows from Eq. (11) that the rate of the reemission of spontaneous photons by the atom is given by the expression

$$\frac{dn_{ph}}{dt} \cong \alpha^2\frac{\omega_r\delta t_p}{\exp(\delta t_p)}. \quad (12)$$

Since each reemission event increases the kinetic energy by a value larger than the height of the localizing potential, the atom localization time interval is equal to $\tau_{trap} \approx (dn_{ph}/dt)^{-1}$.

For the Rb atom and the above-presented parameters of the laser field, the atom localization time interval

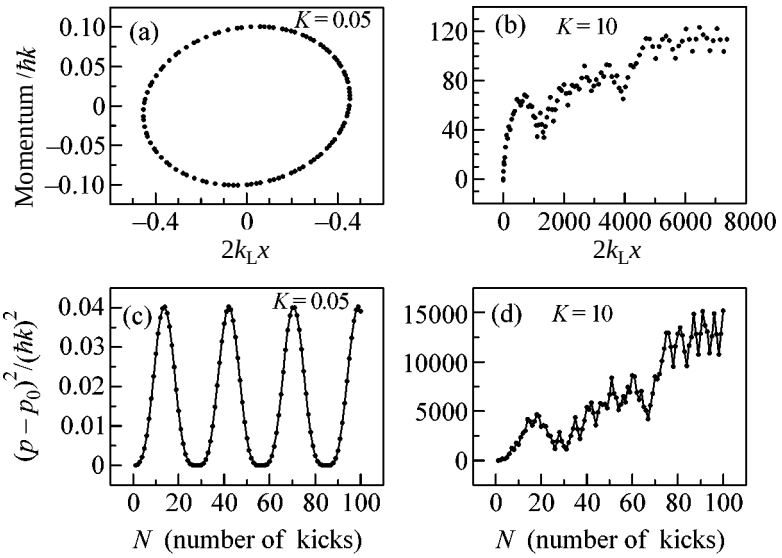

Fig. 2. (a, b) Trajectories of the atom on the phase plane (x, ρ) in the field of femtosecond laser pulses for the stochasticity parameter $K = 0.05$ and 10. (c, d) Mean momentum squared vs. the number of laser "kicks."

is equal to $\tau_{tr} \approx 0.1\alpha^{-2}$. For the atomic velocity $\vartheta_{at} = v_r$, the localization time is equal to $\tau_{tr} = 0.1$ s, and, for the velocity $\vartheta_{at} = 0.1v_r$, the localization time increases to $\tau_{tr} = 10$ s. The atom localization time interval can be increased by increasing the detuning frequency of the laser field.

It is well known that motion may be chaotic in a system subjected to periodic short kicks [9, 10]. The degree of chaos depends on the stochasticity parameter K. For $K \ll 1$, the motion of the system is almost regular (with regions of local chaos); for $K \sim 1$, the motion of the system is chaotic for most initial conditions; and for $K > 4$, widespread chaos occurs. The stochasticity parameter K in the atom-localization problem is determined by the parameters of the laser field and the atom. It follows from Eqs. (3) and (4) that the stochasticity parameter is expressed as

$$K = (\Omega_R^2/\delta)\omega_r T t_p. \tag{13}$$

The following question arises: is it possible to realize those conditions of the interaction of the laser field under consideration and the atom under which necessary conditions (6) of localization are simultaneously satisfied and, at the same time, the inevitable presence of chaos in the dynamics of the system is not breaking? The quantitative characteristics of the dynamics of the atom subjected to periodic short kicks may be obtained using the standard mapping technique [9]. The classical equations of motion of the atom in the potential specified by Eqs. (3) and (4),

$$\dot{X} = P/M, \tag{14a}$$

$$\dot{P} = \partial V/\partial t, \tag{14b}$$

reduce to the standard mapping [9, 10]

$$x_{n+1} = x_n + \rho_{n+1}, \tag{15a}$$

$$\rho_{n+1} = \rho_n + K\sin x_n, \tag{15b}$$

where $x = 2k_L X$ and $\rho = 2k_L(P/M)T$ are the dimensionless coordinate and momentum, respectively.

Figure 2 shows examples of the atomic trajectories on the phase plane (x, ρ) in the field of femtosecond pulses for two stochasticity parameters $K = 0.05$ and 10. For the small stochasticity parameter $K = 0.05$, the motion is finite (Fig. 2a), and chaos is observed for the larger stochasticity parameter $K = 10$ (Fig. 2b). The atom undergoes 100 kicks. Figure 2 also shows the mean velocity squared of the atom as a function of interaction time interval (number of kicks) as calculated from the expression

$$(\rho - \rho_0)^2 = K^2 \sum_{i}^{n-1} \sum_{j}^{n-1} \sin x_i \sin x_j. \tag{16}$$

As is seen in Fig. 2, the motion of the atom remains bounded at the small stochasticity parameter ($K = 0.05$), and the atomic velocity increases unboundedly at the large stochasticity parameter ($K = 10$). Computer calculation is impossible for an interaction time of about 1 s (expected atomic lifetime), because this calculation corresponds to about 10^8 kicks.

The degree of chaos in the motion of the atom at a large number of kicks can be estimated by considering the problem quantum mechanically. Let $|\psi(k)\rangle$ be the state vector before the kth kick. After the kick, the state vector of the atom is

$$\exp[-iV(kT)t_p/\hbar]|\psi(k)\rangle, \tag{17}$$

where $V(kT)$ is the interaction potential at time $t = kT$. The dynamics of the atom between kicks is governed by the operator $\exp[-iH_0t/\hbar]$. Therefore, the atomic state before the $(k+1)$th kink is related to the atomic state before the kth kink as

$$|\psi(k+1)\rangle = \exp(-iH_0T/\hbar) \times \exp[-iV(kT)t_p/\hbar]|\psi(k)\rangle. \quad (18)$$

With the use of the following expansion of the state vector $|\psi(k)\rangle$ in the eigenvectors $|\psi_m\rangle$ of the unperturbed operator H_0,

$$|\psi(k)\rangle = \sum_m c_m(k)|\psi_m\rangle, \quad (19)$$

the quantum map is represented as

$$c_n(k+1) = \sum_m V_{nm}(k)c_m(k). \quad (20)$$

Quantum map (20) relates the coefficients of the expansion of the state vector $|\psi(k+1)\rangle$ before the $(k+1)$th kink to the respective coefficients before the kth kink.

For the case under consideration, the transformation matrix $V_{nm}(k)$ has the form

$$V_{nm}(k) = (-i)^{n-m}J_{n-m}[\Omega_{\text{eff}}(kT)t_p] \times \exp(-i\hbar m^2\omega_r T/2), \quad (21)$$

where J_{n-m} is the Bessel function of the first kind of the $(n-m)$th order and $\Omega_{\text{eff}} = \Omega_R^2/\delta$ is the effective Rabi frequency. The coefficients c_m in Eq. (20) govern the time variation of the momentum of the atom:

$$\langle p\rangle = \sum_{n=-N}^{n=N} n|c_n(k)|^2. \quad (22)$$

Analogously to the classical consideration, the calculation of $\langle p\rangle$ is impossible because of the huge number of kinks for the expected lifetime of the atom in the trap. However, momentum change can be estimated for the case where the atomic momentum changes insignificantly during one kink. The coefficients c_n in Eq. (22) depend on the Bessel function value $J_{n-m}(\Omega_{\text{eff}}t_p)$ in expression (21) for the transformation matrix elements. For a small argument ($\Omega_{\text{eff}}t_p \ll 1$), the Bessel function may be approximated as

$$J_l(\Omega_{\text{eff}}t_p) \approx \frac{1}{2^l l!}(\Omega_{\text{eff}}t_p)^l. \quad (23)$$

An increase in the momentum can be estimated considering the case where the atom is initially quite well localized ($v_{at} < v_r$). Using the complete set of eigenstates in which $\langle x|\psi_m\rangle = (1/\sqrt{2\pi\hbar})\exp(ipx/\hbar)$ and the initial state $|\psi_0\rangle = |p = 0\rangle$, one can conclude that the probability of populating the neighboring state $|\psi_1\rangle = |p = \hbar k\rangle$ after one kick is equal to

$$P = |J_1(\Omega_{\text{eff}}t_p)|^2 \approx \frac{1}{4}(\Omega_{\text{eff}}t_p)^2. \quad (24)$$

When the probability of populating the neighboring state after the action of N laser pulses becomes equal to unity, the atom can be treated as completely delocalized. From this condition, the atomic lifetime in the trap is estimated as

$$t_{\text{trap}} \approx \frac{T}{t_p^2}\frac{\delta^2}{\Omega_R^4}. \quad (25)$$

For the following parameters of the laser pulse, $t_p = 3.5\times10^{-15}$ s, $\Omega_R = 2\pi\alpha 5\times10^{11}$ s^{-1}, and $\delta = 2\pi\times10^{14}$ s^{-1}, the atomic lifetime is equal to $t_{\text{trap}} \sim 2.5\times10^3/\alpha^4$ s. For $\alpha \le 1$, this value is much longer than the spontaneous-decay lifetime of the atom.

I am grateful to H. Takuma and P.N. Melent'ev for stimulating discussions of the results. This work was supported in part by INTAS (grant no. INFO 00-479), the US Civilian Research and Development Foundation for the Independent States of the Former Soviet Union (grant no. RU-P1-2572-TR-04) and the Ministry of Education, Science, Sport, and Culture of Japan.

REFERENCES

1. W. D. Phillips, Rev. Mod. Phys. **70**, 721 (1998).
2. S. Chu, Rev. Mod. Phys. **70**, 685 (1998).
3. C. N. Cohen-Tannoudji, Rev. Mod. Phys. **70**, 707 (1998).
4. C. S. Adams and E. Riis, Prog. Quantum Electron. **21**, 1 (1997).
5. R. Grimm, M. Weidemüller, and Y. B. Ovchinnikov, Adv. At. Mol. Opt. Phys. **42**, 95 (2000).
6. V. I. Balykin, V. G. Minogin, and V. S. Letokhov, Rep. Prog. Phys. **63**, 1429 (2000).
7. H. Karori, T. Ido, and M. Kawata-Gonokami, J. Phys. Soc. Jpn. **68**, 2479 (1999).
8. H. Karori, M. Takamoto, V. G. Palchikov, and V. D. Ovsiannikov, Phys. Rev. Lett. **91**, 173005 (2003).
9. B. V. Chirikov, Phys. Rep. **52**, 265 (1965).
10. M. G. Raizen, Adv. Mol. Opt. Phys. **41**, 43 (1999).
11. T. Brabec and F. Krausz, Rev. Mod. Phys. **72**, 545 (2000).
12. J. Chang and J. Zhou, Phys. Rev. A **67**, 041404(R) (2003).
13. R. Graham, M. Schlautmann, and P. Zoller, Phys. Rev. A **45**, R19 (1992).
14. R. Netz, T. Feurer, G. Robert, and R. Sauerbreg, Phys. Rev. A **65**, 043406 (2002).
15. P. W. Milloni, J. P. Ackerhalt, and M. E. Goggin, Phys. Rev. A **35**, 1714 (1987).

Translated by R. Tyapaev

JETP Letters, Vol. 81, No. 5, 2005, pp. 214–217. Translated from Pis'ma v Zhurnal Éksperimental'noĭ i Teoreticheskoĭ Fiziki, Vol. 81, No. 5, 2005, pp. 274–277.

Propagation of Whistlers in a Plasma with a Magnetic Field Duct

M. E. Gushchin, S. V. Korobkov, A. V. Kostrov, A. V. Strikovsky, and T. M. Zaboronkova

Institute of Applied Physics, Russian Academy of Sciences, ul. Ul'yanova 46, Nizhni Novgorod, 603950 Russia

e-mail: mguschin@appl.sci-nnov.ru

Received January 31, 2005

The propagation of whistlers in a homogeneous magnetized plasma in the presence of a magnetic field duct has been experimentally investigated. The possibility of efficiently trapping whistlers in a narrow (wavelength-scale) cylindrical duct with the increased field has been demonstrated. It has been shown that a comparatively slight perturbation of the external magnetic field ($\delta B/B_0 \sim 0.1$) can significantly change the spatial structure and increase the amplitude of whistlers near the duct axis. © *2005 Pleiades Publishing, Inc.*

PACS numbers: 52.25.Xz, 52.35.Hr, 52.72.+v

The ducting of whistlers plays a key role in the propagation of signals of very low frequencies in the near-Earth plasma. The presence of plasma inhomogeneities (ducts) that are extended along the geomagnetic field lines is of fundamental importance for magnetospheric physics, because it provides an explanation of the efficient transfer of low-frequency radiation between the magnetic conjugate points of the ground. Only ducts with increased or decreased plasma density are traditionally considered [1]. The propagation of whistlers in density ducts has been well studied both theoretically [2] and experimentally [3]. Owing to nonlinear thermal effects in the near field of antennas, artificial waveguide ducts can be formed, which make it possible to control the radiation pattern of high-power transmitters [4, 5].

However, as has been shown in this work, magnetic field inhomogeneities arising when the magnetosphere is disturbed by intense magnetohydrodynamic waves due either to the diamagnetism of hot particles of the Earth's radiation belts or to phenomena that are similar to the inverse Faraday effect [6], which can be observed when intense elliptically polarized waves propagate in the plasma, can significantly affect the propagation of whistlers ($\sqrt{\omega_H \Omega_H} < \omega < \omega_H \ll \omega_p$, where ω is the wave frequency, ω_p is the plasma frequency, and ω_H and Ω_H are the cyclotron frequencies of electrons and ions, respectively). The possibility of the trapping of whistlers in magnetic field ducts was pointed out in [2, 7], and certain properties of magnetic field ducts were discussed in [8].

In this work, the propagation of whistlers in a cylindrical duct with an increased or decreased magnetic field that is created in a homogeneous plasma is experimentally studied at the Krot setup. The effect of the transverse inhomogeneity of the magnetic field on the spatial structure of wave fields that are created in the plasma has been analyzed.

The experimental setup was a vacuum chamber 10 m long and 3 m in diameter (Fig. 1a). The magnetic field of the mirror configuration (mirror ratio $R = 2.4$, Fig. 1b) was created by means of a solenoid that was mounted inside the vacuum chamber (this solenoid is not shown in Fig. 1). In the experiment, the magnetic field in the central section of the chamber was equal to $B_0 = 35$ G. The cylindrical plasma column (with a length of 4 m and a diameter of 1.5 m) was formed due to the pulsed inductive rf discharge ($f_{\text{dis}} = 5$ MHz,

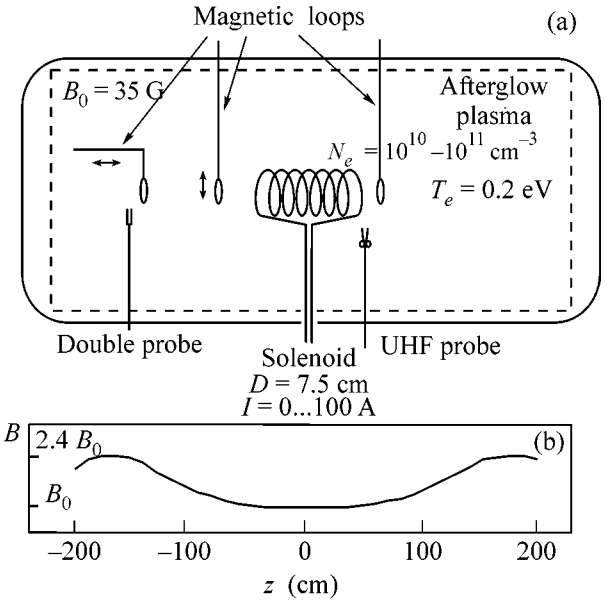

Fig. 1. (a) Scheme of the Krot experimental setup and (b) magnetic field distribution along the vacuum-chamber axis.

0021-3640/05/8105-0214$26.00 © 2005 Pleiades Publishing, Inc.

$P_{gen} \sim 250$ kW, $\tau_{pulse} = 1$ ms) in argon at a pressure of $p = 7 \times 10^{-4}$ Torr. The maximum plasma density at the discharge time was on the order of 10^{13} cm^{-3}, the electron temperature was equal to $T_e \sim 10$ eV, and the ion temperature was $T_i \leq 0.5$ eV. Plasma decay was determined by the ambipolar diffusion of electrons along the magnetic field.

Experiments were carried out in a decaying quiescent plasma within the interval 6–12 ms after the plasma-creating generators had been turned off. Over the indicated time interval, the plasma density monotonically varied from 10^{11} to 2×10^{10} cm^{-3} at electron temperatures $T_e \leq 0.2$ eV.

The transverse inhomogeneity of the magnetic field (magnetic duct) was created by means of a cylindrical seven-coil solenoid situated at the center of the chamber (coil diameter $D = 7.5$ cm and distance between coils $l = 5.5$ cm, Fig. 1a). The solenoid was made of an insulated copper wire with a diameter of $d = 1$ mm. A current of $I_{max} = 100$ A in the form of a rectangular pulse of duration of $\tau = 0.2$–1 ms passed through the solenoid. The propagation of whistlers in the duct with the increased and decreased magnetic field was studied. The form of the duct was determined by the polarity of the connection of the solenoid to a supply source.

Measurements of density that were carried out by a microwave resonator probe [9] showed that the introduction of a solenoid into the plasma volume did not give rise to a significant redistribution of the plasma (Fig. 2). The deposition of particles on the wire and supporting structures of the solenoid leads to a decrease in the electron density by no more than 7–10% at a scale much larger than the coil diameter. Moreover, no change is observed in the density when a pulse current up to 100 A flows through the solenoid.

The excitation and reception of rf whistlers ($f = \omega/2\pi = 20$–50 MHz, $P < 1$ W) were performed by means of magnetic loop antennas 1 cm in diameter that were placed in various sections of the plasma column. In order to reduce the plasma effect on the impedance characteristics of the antennas, they were coated with a thin dielectric film. Interferometric measurements showed that the antennas excited oblique whistlers in the plasma with wavelengths $\lambda_\parallel \sim \lambda_\perp \sim 15$–$30$ cm in the indicated parameter range. In experiments, a transmitting antenna was placed on the axis of the system at a distance of $z = 5$ cm from the extreme coil of the solenoid. The transverse structure of the rf field was analyzed by means of a diagnostic antenna, which was freely displaced over a radius in a plane that was spaced 7 cm from the opposite end of the solenoid. Signals from the plasma were detected by a receiver with a band of $\Delta f = 100$ kHz.

Figure 3 shows the transverse distributions of the amplitude of a probe wave with an amplitude of $f = 20$ MHz in the plasma (*1*) with an unperturbed magnetic field and in the presence of the (*2*) increased and

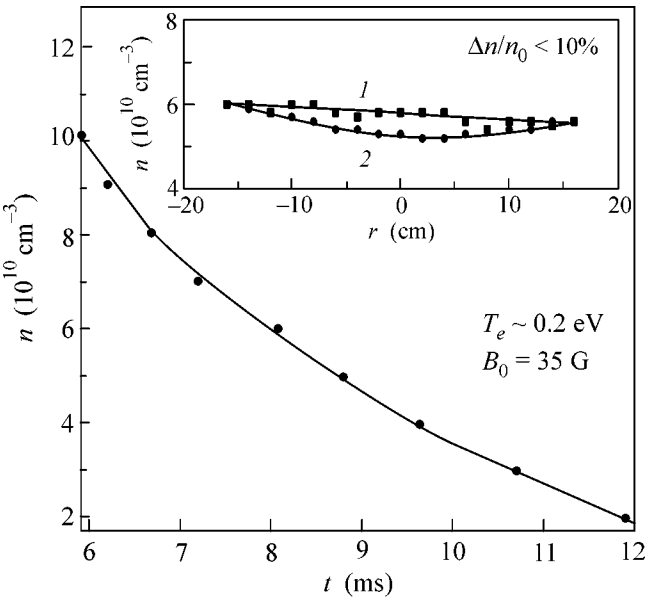

Fig. 2. Time dependence of the density of the decaying plasma. The inset shows the transverse distribution of the plasma density at 8 ms after the plasma-creating generator has been turned off (*1*) in the absence of a solenoid and (*2*) in the presence of the solenoid that was introduced into the plasma volume and that created a magnetic duct (solenoid diameter is $D = 7.5$ cm).

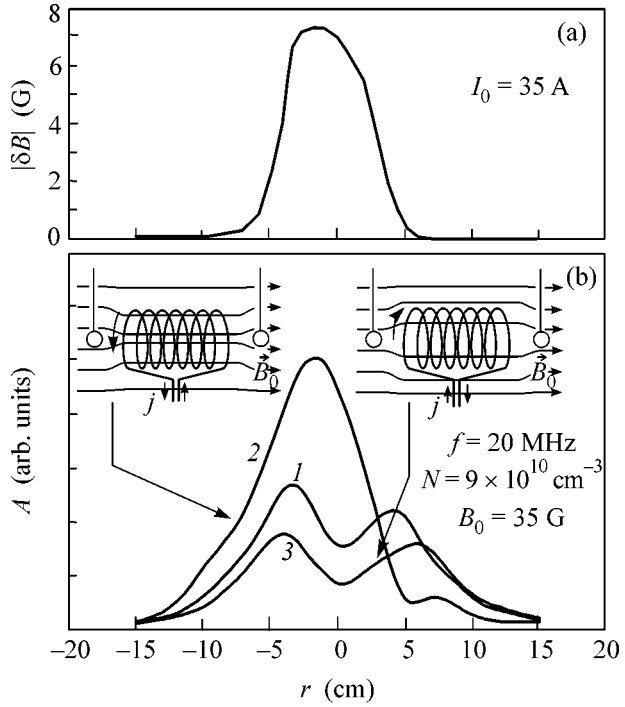

Fig. 3. Transverse distributions of (a) the magnetic field created by the solenoid and (b) the amplitude of an rf whistler ($f = 20$ MHz) in the homogeneous plasma (*1*) in the absence of a duct and at the exit of the duct with the (*2*) increased and (*3*) decreased magnetic fields (the relative perturbation of the magnetic field in the duct is $\delta B/B_0 = 0.2$).

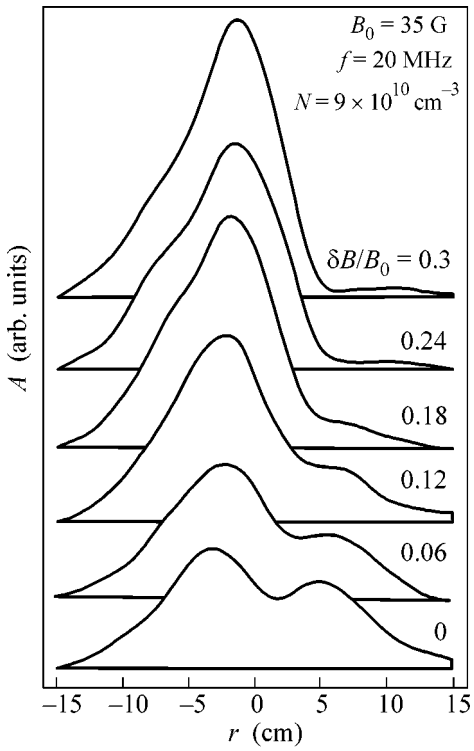

Fig. 4. Transverse distributions of the rf field of the whistler (f = 20 MHz) propagating in the duct with the increased magnetic field for various perturbations of the magnetic field in the duct.

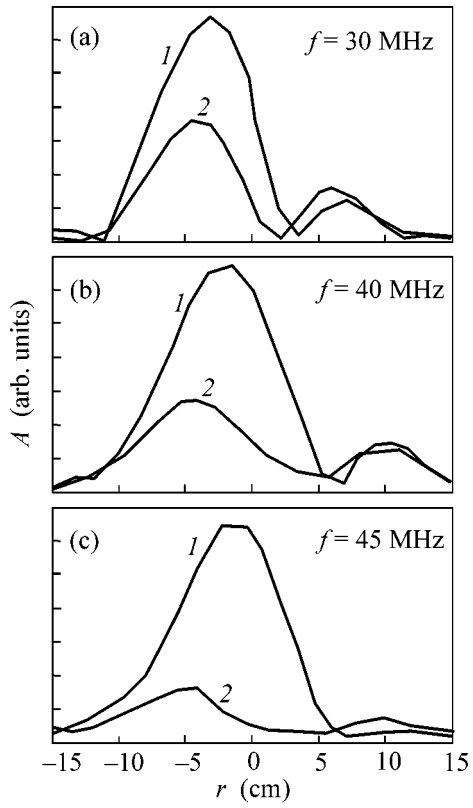

Fig. 5. Transverse distributions of rf wave fields (*1*) in the presence of the duct with an increased magnetic field (relative perturbation of the magnetic field in the duct is $\delta B/B_0$ = 0.1) and (*2*) in the absence of the duct for the parameters $N = 4 \times 10^{10}$ cm^{-3} and B_0 = 35 G and for various frequencies.

(*3*) decreased magnetic fields. The relative perturbation of the magnetic field was $|\delta B|/B_0 = 0.2$. In the presence of the decreased-field duct, the amplitude of the received signal decreases, and the transverse distribution of the rf field was broader than the distribution of the wave field in the absence of the duct. At the same time, the creation of the duct with the increased magnetic field changed the spatial structure and caused a significant increase in the amplitude of the rf field near the duct axis. In the latter case, a whistler was efficiently trapped in the magnetic duct, and the propagation of waves in the increased-field duct was investigated in detail in the experiment.

Figure 4 shows the redistribution of the rf field (f = 20 MHz) when the current in the solenoid increases from 0 to 50 A. Note that the structure of rf fields changed even for a comparatively small perturbation of the magnetic field at $\delta B/B_0 = 0.1$. When the magnetic field in the duct increased to $\delta B/B_0 = 0.3$, the amplitude of the rf field was almost tripled, and the field was localized near the duct axis.

The transverse distributions of the amplitudes of waves with various frequencies that are emitted into the duct with the increased magnetic field are shown in Fig. 5. The results were obtained for a fixed small perturbation ($\delta B/B_0 = 0.1$) of the magnetic field. As frequency increases, the difference between the structures and amplitudes of fields in the presence and absence of the duct becomes more pronounced. The trapping of whistlers is particularly efficient at frequencies $f \lesssim f_H/2$, where $f_H = \omega_H/2\pi \simeq 100$ MHz (f = 45 MHz, Fig. 5c).

In order to explain the experimental results, we analyze the dispersion properties of whistlers. The dispersion relation for whistlers has the form

$$n = \frac{kc}{\omega} = \frac{\omega_p}{\sqrt{\omega(\omega_H \cos\Theta - \omega)}}, \qquad (1)$$

where n is the refractive index of the whistler, k is the wavenumber, c is the speed of light in vacuum, and Θ is the angle between the wave vector and the external magnetic field. According to Eq. (1), under the condition $\omega \ll \omega_H \cos\Theta$, the properties of magnetic field ducts for the propagation of whistlers are similar to the waveguide characteristics of plasma-density ducts [7]. In particular, for low frequencies, ducts with the increased field are equivalent to lowered-density ducts, which efficiently confine oblique whistlers with $\lambda_\parallel \sim \lambda_\perp$ [3]. However, when the frequency approaches half the electron gyrofrequency, the analog between density

ducts and magnetic field ducts is broken. For whistlers, the curvature of the wave vector surface for frequencies $\omega \sim \omega_H/2$ is very small, and even a small change in the ratio ω/ω_H in the duct can lead to a strong change in the conditions of the propagation and trapping of waves. Under these conditions, small (10%) transverse variations in the magnetic field significantly affect the spatial structure of rf fields. This conclusion is corroborated in the experiment (Fig. 5c).

Let us discuss certain features of the experimental procedure. First, the longitudinal length of the whistler wave exceeds the diameter of the magnetic field duct in the experiment. Hence, the geometrical optics approach [7] can be used only for qualitative analysis of the conditions of the trapping of whistlers in the duct. Second, no more than two or three wavelengths are kept in the length of the created duct. Under these conditions, the diffraction of the whistler on the magnetic field inhomogeneity whose size is comparable to the wavelength takes place rather than the excitation of the eigenmodes of the magnetic duct. The investigation of duct modes would be possible for a longer duct.

In conclusion, we discuss the conditions for the existence of magnetic field ducts in the near-Earth plasma. In particular, it is known that, in addition to the cold ($T_e \sim T_i \sim 1$ eV) background plasma with density n_0 in the inner magnetosphere, there is a small fraction ($n_{\text{hot}} < 10^{-3} n_0$) of "hot" electrons and protons (in the radiation belts and ring-current region) with energies above 10 keV [10]. Despite an extremely low density of the hot component, its energy increases strongly under the conditions of strong geomagnetic disturbances. In this case, the following condition can be valid [11]:

$$n_{\text{hot}} T_{\text{hot}} \leq \frac{B^2}{8\pi}, \qquad (2)$$

where T_{hot} is the temperature of the hot particles and $B^2/8\pi$ is the energy density of the geomagnetic field. In this case, the azimuthal inhomogeneity of the density and temperature of energetic particles can give rise to strong diamagnetic disturbances, which are not accompanied by variations in the density of the cold background plasma. Moreover, the channeling formations can have the dynamic character, and whistlers can be trapped in inhomogeneities created by intense, extremely low frequency oscillations (magnetic pulsations) whose amplitude reaches $\delta B \sim 10$ nT [12] (relative field perturbation $\delta B/B \sim 5$–10%).

Thus, the laboratory experiments and estimates show that the transverse inhomogeneities of the Earth's magnetic field can serve as ducts for whistlers, particularly during periods of strong disturbance of the magnetosphere.

This work was supported by the Russian Foundation for Basic Research (project nos. 04-02-17188 and 04-02-16344), the Russian Department of Science (Program for the Support of Unique Setups, project no. 01-18), and the Council of the President of the Russian Federation for Support of Young Russian Scientists and Leading Scientific Schools (project no. NSh-1639.2003.02).

REFERENCES

1. J. C. Cerisier, J. Atmos. Terr. Phys. **36**, 1443 (1974).
2. I. G. Kondrat'ev, A. V. Kudrin, and T. M. Zaboronkova, *Electrodynamics of Density Ducts in Magnetized Plasmas* (Gordon and Breach, Amsterdam, 1999).
3. M. T. Zaboronkova, A. V. Kostrov, A. V. Kudrin, *et al.*, Zh. Éksp. Teor. Fiz. **102**, 1151 (1992) [Sov. Phys. JETP **75**, 625 (1992)].
4. R. L. Stenzel, Phys. Fluids **19**, 857 (1976).
5. A. V. Kostrov, A. I. Smirnov, M. V. Starodubtsev, and A. A. Shaĭkin, Pis'ma Zh. Éksp. Teor. Fiz. **67**, 548 (1998) [JETP Lett. **67**, 579 (1998)].
6. L. P. Pitaevskiĭ, Zh. Éksp. Teor. Fiz. **39**, 1450 (1960) [Sov. Phys. JETP **12**, 1008 (1961)].
7. R. N. Kaufman, Izv. Vyssh. Uchebn. Zaved., Radiofiz. **27**, 1102 (1984).
8. W. Calvert, J. Geophys. Res. **100**, 17491 (1995).
9. I. G. Kondrat'ev, A. V. Kostrov, A. I. Smirnov, *et al.*, Fiz. Plazmy **28**, 977 (2002) [Plasma Phys. Rep. **28**, 900 (2002)].
10. R. H. W. Friedel and A. Korth, Adv. Space Res. **20**, 311 (1997).
11. L. R. Lyons and D. J. Williams, *Quantitative Aspects of Magnetospheric Physics* (Reidel, Dordrecht, 1984; Mir, Moscow, 1987).
12. T. A. Plyasova-Bakounina, J. Kangas, K. Mursula, *et al.*, J. Geophys. Res. **101**, 10965 (1996).

Translated by R. Tyapaev

JETP Letters, Vol. 81, No. 5, 2005, pp. 218–221. Translated from Pis'ma v Zhurnal Éksperimental'noĭ i Teoreticheskoĭ Fiziki, Vol. 81, No. 5, 2005, pp. 278–282.

Applicability Conditions for the Dipole Approximation in the Problems of Scattering of Surface Plasmon Polaritons

A. B. Evlyukhin[1] and S. I. Bozhevolnyi[2]

[1] *Vladimir State University, Vladimir, 600000 Russia*
e-mail: a.b.evlyukhin@mail.ru
[2] *Aalborg University, DK-9220 Aalborg ø, Denmark*

Received January 21, 2005

Using the method of the tensor Green's function of the wave equation, the conditions have been determined under which the dipole approximation is sufficient in the problem of the scattering of surface optical electromagnetic waves (surface plasmon polaritons) on a small spherical particle. The independence of the electric field inside the scatterer of the spatial coordinates is used as the main requirement of the dipole approximation. Conditions are obtained in the form of inequalities involving the wavenumber, the material parameters of the system, and the size of the scatterer and its position with respect to the surface on which plasmon polaritons are excited. © *2005 Pleiades Publishing, Inc.*

PACS numbers: 02.70.–c, 03.65.Nk, 71.36.+c, 78.68.+m

Investigation of surface optical electromagnetic waves, which arise at the interface between a dielectric and a metal and decay exponentially with the distance from the interface, is of great interest at present [1, 2]. Free charge carriers of the metal are predominantly involved in the generation of these waves. For this reason, these waves are often called surface plasmon polaritons (SPPs). There are two reasons for this particular increased interest. First, the invention and development of near-field optical microscopy provided the possibility of directly observing SPPs immediately near the surface and, hence, of not only investigating their properties but also directly affecting the process of their excitation. Second, significant advances in nanotechnologies have enabled researchers to control the process of the propagation and scattering of SPPs at length scales much less than the length of their damping caused by absorption in the metal. Therefore, methods for the concentration and directional propagation of light energy in microsystems with sizes of about a wavelength of light or smaller can be experimentally studied using the properties of SPPs.

For a clear breakthrough in this direction, it is necessary to perform numerous theoretical investigations of the processes of the scattering of SPPs on various objects. This is a very intricate problem that requires numerical calculations even in a relatively simple case of a single symmetric scatterer [3]. For this reason, when analyzing the multiple scattering of SPPs in systems containing numerous scatterers, one is forced to use a number of approximations that make it possible to describe the scattering of SPPs by a separate object using a relatively simple method. The application of the dipole approximation is one such approach. Moreover, the propagation of SPPs in various surface structures with a finite number of scatterers has been numerically simulated only in this approximation [4–7]. However, open questions concerning the applicability limit for this approximation in the problem of the scattering of SPPs exist to date. Two restrictions on the scatterer size are often given as sufficient conditions. First, the scatterer must be much smaller than the wavelength of the external field, and, second, the distance from it to the surface with SPPs must be much larger than its size. These two conditions are justified. However, as has been shown in this work, they must generally be supplemented by additional requirements that include the relations between the material and configuration parameters of the system.

In order to analyze the scattering of SPPs, we apply the method of the tensor Green's function of the wave equation [8]. The advantage of this method is that it enables one to independently consider different scattering channels for SPPs from the very beginning. Such a possibility follows from the representation [9] recently obtained for the Green's tensor of the system of two half-spaces that are filled with a metal and a dielectric with a planar interface. This representation is a sum of several terms, each describing excitation in the system of electromagnetic fields of a certain type: quasi-static or near-zone electric field, field of SPPs, and transverse electromagnetic waves propagating from the metal surface to the far wave zone. We emphasize that the decomposition of the Green's tensor into the above terms may be strictly performed only when the absorption of electromagnetic energy in the metal is disregarded [9]. For this reason, here we assume that the dielectric constants of the system without the scatterer

are real. This assumption is justified because, for noble metals that are primarily used in experiments with surface electromagnetic waves of the visible or infrared range, the damping length for SPPs is several times longer than their wavelength [2]. Therefore, damping is immaterial when the properties of SPPs are studied at the scale of their wavelength.

We consider a surface plane electromagnetic wave that has frequency ω and propagates along the planar interface between two half-spaces filled with metal and dielectric with dielectric constants ε_m and ε_d, respectively, such that $-\varepsilon_m > \varepsilon_d$. Under this condition, the existence of SPPs is possible. A SPP wave is scattered by a macroscopic spherical particle that is situated at the interface on the dielectric side. This particle has radius R_p and dielectric constant ε_p. The position of the particle is given by the radius vector $\mathbf{r}_p$ with coordinates $(0, 0, z_p)$ in the Cartesian coordinate system, where z_p is the distance between the center of the particle and the metal–dielectric interface. The total electromagnetic field in the system satisfies Maxwell's equations

$$\nabla \times \mathbf{E} = i\omega\mu_0\mathbf{H}, \tag{1}$$

$$\nabla \times \mathbf{H} = -i\omega\varepsilon_0\varepsilon\mathbf{E} - i\omega\Theta(R_p - |\mathbf{r} - \mathbf{r}_p|)\mathbf{P}, \tag{2}$$

where $\mathbf{E}$ and $\mathbf{H}$ are the electric and magnetic fields, respectively; μ_0 is the permeability of free space; ε_0 is the permittivity of free space; $\Theta(R_p - |\mathbf{r} - \mathbf{r}_p|)$ is the Heaviside step function; $\mathbf{P} = \varepsilon_0(\varepsilon_p - \varepsilon_d)\mathbf{E}(\mathbf{r})$ is the particle polarization vector; and ε is the dielectric constant of the system without the scatterer. In terms of the method of the tensor Green's function, the total electric field beyond the particle at distances $|\mathbf{r} - \mathbf{r}_p| \gg R_p$ in the dipole approximation is determined by the equation

$$\mathbf{E}(\mathbf{r}) = \mathbf{E}_0(\mathbf{r}) + \frac{k_0^2}{\varepsilon_0}\hat{G}(\mathbf{r}, \mathbf{r}_p)\mathbf{p}. \tag{3}$$

Here, $\mathbf{E}_0(\mathbf{r})$ is the electric field of the external (incident) SPP wave, k_0 is the wavenumber in vacuum, $\hat{G}(\mathbf{r}, \mathbf{r}')$ is the Green's tensor of the system without the scatterer, and the electric dipole moment of the particle $\mathbf{p}$ is given by the expression

$$\mathbf{p} = \varepsilon_0(\varepsilon_p - \varepsilon_d)\int_{V_p}\mathbf{E}(\mathbf{r})d\mathbf{r}, \tag{4}$$

where $V_p = 4\pi R_p^3/3$ is the volume of the particle. The dipole approximation describes the basic contribution to scattering if the electric field inside the particle is uniform. In this case, the dipole moment is equal to $\mathbf{p} = \varepsilon_0(\varepsilon_p - \varepsilon_d)V_p\mathbf{E}(\mathbf{r}_p)$, where the electric field is taken at the center of the particle for the sake of definiteness.

Let us find the electric field inside the particle and determine the conditions under which this field can be treated as uniform. In order to determine the electric field inside the particle, we consider the Lippmann–Schwinger integral equation

$$\mathbf{E}(\mathbf{r}) = \mathbf{E}_0(\mathbf{r}) + \frac{k_0^2}{\varepsilon_0}\int_{V_p}\hat{G}(\mathbf{r}, \mathbf{r}')\mathbf{P}(\mathbf{r}')d\mathbf{r}', \tag{5}$$

where $\mathbf{r} \in V_p$. The Green's tensor is represented as the following sum of several terms responsible for the excitation of electromagnetic fields of certain types in the system [9]:

$$\begin{aligned}\hat{G}(\mathbf{r}, \mathbf{r}') = {} & \hat{G}_q^0(\mathbf{r}, \mathbf{r}') + \hat{G}_q^s(\mathbf{r}, \mathbf{r}') + \hat{G}_T^0(\mathbf{r}, \mathbf{r}') \\ & + \hat{G}_T^s(\mathbf{r}, \mathbf{r}') + \hat{G}_{\text{SPP}}(\mathbf{r}, \mathbf{r}').\end{aligned} \tag{6}$$

Here, the excitation of the quasi-static field in the system is described by the terms $\hat{G}_q^0$ and $\hat{G}_q^s$, the latter of which includes the effect of the interface between two media; the excitation of transverse fields in the system is described by terms the $\hat{G}_T^0$ and G_T^s, the latter of which includes the effect of the metal–dielectric interface; and $\hat{G}_{\text{SPP}}$ corresponds to the excitation of SPPs in the system.

Our approach is based on the well-known solution to the problem of the scattering of electromagnetic waves on a small particle in uniform space (Rayleigh theory) [10]. In this case, the electric dipole approximation makes the basic contribution to the scattered field if the solution to the quasi-stationary problem is sufficient for determining the electric field inside the particle. Under this condition, the field inside the particle is uniform, and its electric dipole moment can be simply calculated. In terms of the Green's function, this means that, when the Lippmann–Schwinger equation is solved for the particle volume and the near-field zone, the external field $\mathbf{E}_0$ can be treated as uniform, and it is sufficient to approximate the Green's function by its quasi-static part $\hat{G}_q^0(\mathbf{r}, \mathbf{r}')$. In this case, the electric field inside the particle is given by the expression

$$\mathbf{E} = \frac{3\varepsilon_h}{\varepsilon_p + 2\varepsilon_h}\mathbf{E}_0, \tag{7}$$

where ε_h is the dielectric constant of the homogeneous medium. If the particle is situated near the planar interface between two media, in order for the quasi-static electric field in the particle to be treated as uniform, an additional condition must be satisfied; namely, the distance between the particle and interface must be much larger than the particle size ($R_p \ll z_p$). Indeed, in this case, the quasi-static effect of the interface on the field in the particle can be taken into account by the image method of introducing a certain effective electric dipole, i.e., an image of the dipole corresponding to the particle. The electric field that the image creates at the place where the particle is located is nearly uniform due to the condition $R_p \ll z_p$. Therefore, one can say that the

particle is subjected to uniform external electric fields, and the field inside the particle is also uniform under these conditions. Thus, the dipole approximation is sufficient for describing the scattering of SPPs on the small particle if the quasi-static approximation of Green's function (6) is sufficient for determining the field inside the particle and if $R_p \ll z_p$ and $R_p k_s \ll 1$, where $k_s = k_0\sqrt{\varepsilon_d\varepsilon_m/(\varepsilon_d+\varepsilon_m)}$ is the wavenumber of the SPP.

Assuming that the field inside the particle is independent of the spatial coordinates, we express it from Eq. (5):

$$\mathbf{E}(\mathbf{r}_p) \approx \frac{3\varepsilon_d}{\varepsilon_p+2\varepsilon_d}\left[\hat{\mathbf{I}} - \frac{k_0^2}{\varepsilon_0}\alpha_0\left\{\hat{G}_q^s(\mathbf{r}_p,\mathbf{r}_p) + \frac{1}{V_p}\int_{V_p}[\hat{G}_T^0(\mathbf{r}_p,\mathbf{r}) + \hat{G}_T^s(\mathbf{r}_p,\mathbf{r}) + \hat{G}_{\mathrm{SPP}}(\mathbf{r}_p,\mathbf{r})]d\mathbf{r}\right\}\right]^{-1}\mathbf{E}_0(\mathbf{r}_p), \tag{8}$$

where $\hat{\mathbf{I}}$ is the 3×3 identity tensor and $\alpha_0 = 3\varepsilon_0\varepsilon_d V_p(\varepsilon_p-\varepsilon_d)/(\varepsilon_p+2\varepsilon_d)$ is the quasi-static polarizability of the small spherical particle. In Eq. (8), the field is taken for definiteness at the center of the particle and the approximation

$$\int_{V_p}\hat{G}_q^s(\mathbf{r}_p,\mathbf{r})d\mathbf{r} \approx V_p\hat{G}_q^s(\mathbf{r}_p,\mathbf{r}_p) \tag{9}$$

is used under the condition $R_p \ll z_p$. The tensor $\hat{G}_q^s(\mathbf{r}_p,\mathbf{r}_p)$ can be obtained by the electrostatic image method [6, 11] in the form

$$\hat{G}_q^s(\mathbf{r}_p,\mathbf{r}_p) = \frac{\varepsilon_m-\varepsilon_d}{\varepsilon_m+\varepsilon_d}\frac{1}{4\pi k_0^2\varepsilon_d z_p^3}\left(\frac{1}{8}\hat{x}\hat{x}+\frac{1}{8}\hat{y}\hat{y}+\frac{1}{4}\hat{z}\hat{z}\right), \tag{10}$$

where $\hat{x}$, $\hat{y}$, and $\hat{z}$ are the unit vectors of the chosen Cartesian coordinate system. According to Eq. (8), this expression in the quasi-static limit transforms into Eq. (7).

In order to determine the conditions under which the quasi-static part of the Green's function is sufficient for determining the field in the particle, it is necessary to estimate the integrals entering into Eq. (8) and to compare them with the quasi-static contribution. In order to estimate the contribution from transverse fields, we retain only the first term of the expansion of $\hat{G}_T^0(\mathbf{r}_p,\mathbf{r})$ in the small parameter $R_p k_d \ll 1$ ($k_d = k_0\sqrt{\varepsilon_d}$) [12, 13]. In this case, we obtain

$$\int_{V_p}\hat{G}_T^0(\mathbf{r}_p,\mathbf{r})d\mathbf{r} \approx \int_{V_p}\frac{\hat{\mathbf{I}}+\hat{R}\hat{R}}{8\pi R}d\mathbf{r} = \frac{R_p^2}{3}\hat{\mathbf{I}}, \tag{11}$$

where $R = |\mathbf{r}_p - \mathbf{r}|$ and $\hat{R} = \mathbf{R}/R$. Estimating the integral of $\hat{G}_{\mathrm{SPP}}(\mathbf{r}_p,\mathbf{r})$ in Eq. (8), we take into account that this tensor has no singularity at $\mathbf{r} = \mathbf{r}_p$. Therefore, it can be factored out of the integral over the small-particle volume at this point. Then, using a representation for $\hat{G}_{\mathrm{SPP}}(\mathbf{r},\mathbf{r}')$ taken from [9], we obtain

$$\int_{V_p}\hat{G}_{\mathrm{SPP}}(\mathbf{r}_p,\mathbf{r})d\mathbf{r} \approx \frac{V_p k_s a}{(1-a^2)(1-a^4)} \times\left[i\frac{e^{-ak_s 2z_p}}{2} - \mathrm{V.p.}\int_0^\infty\frac{x^2 e^{-xak_s 2z_p}}{\pi(1-x^2)}dx\right] \times\left(\frac{a^2}{2}[\hat{x}\hat{x}+\hat{y}\hat{y}]+\hat{z}\hat{z}\right), \tag{12}$$

where $a = \sqrt{-\varepsilon_d/\varepsilon_m}$ and V.p. means that the principal value is taken for the integral of the expression with a pole singularity. Using Eqs. (10)–(12), from Eq. (8) we obtain conditions under which the quasi-static approximation for the Green's tensor is dominant. Thus, we arrive at the following two conditions associated with transverse waves,

$$\left|1-\frac{(1+a^2)(\varepsilon_p-\varepsilon_d)R_p^3}{8(1-a^2)(\varepsilon_p+2\varepsilon_d)z_p^3}\right| \gg (k_d R_p)^2\left|\frac{\varepsilon_p-\varepsilon_d}{\varepsilon_p+2\varepsilon_d}\right|, \tag{13}$$

$$\left|1-\frac{(1+a^2)(\varepsilon_p-\varepsilon_d)R_p^3}{4(1-a^2)(\varepsilon_p+2\varepsilon_d)z_p^3}\right| \gg (k_d R_p)^2\left|\frac{\varepsilon_p-\varepsilon_d}{\varepsilon_p+2\varepsilon_d}\right|, \tag{14}$$

and the following two conditions associated with the plasmon polariton field,

$$\left|1-\frac{(1+a^2)(\varepsilon_p-\varepsilon_d)}{8(1-a^2)(\varepsilon_p+2\varepsilon_d)}\left(\frac{R_p}{z_p}\right)^3\right| \gg \frac{3}{2}k_0^3 V_p\left|\frac{\varepsilon_p-\varepsilon_d}{\varepsilon_p+2\varepsilon_d}\right|\frac{a^3\varepsilon_d^{3/2}F(ak_s z_p)}{(1-a^2)^{3/2}(1-a^4)}, \tag{15}$$

$$\left|1-\frac{(1+a^2)(\varepsilon_p-\varepsilon_d)}{4(1-a^2)(\varepsilon_p+2\varepsilon_d)}\left(\frac{R_p}{z_p}\right)^3\right| \gg 3k_0^3 V_p\left|\frac{\varepsilon_p-\varepsilon_d}{\varepsilon_p+2\varepsilon_d}\right|\frac{a\varepsilon_d^{3/2}F(ak_s z_p)}{(1-a^2)^{3/2}(1-a^4)}. \tag{16}$$

Here, the function $F(ak_s z_p)$ is given by the expression

$$F = m\frac{e^{-2ak_s z_p}}{2} + n\left|\mathrm{V.p.}\int_0^\infty\frac{x^2 e^{-x2ak_s z_p}dx}{\pi(1-x^2)}\right|, \tag{17}$$

where the two terms arise from the expression in square brackets in Eq. (12). If the first term is equal to or larger than the second term, $m = 1$ and $n = 0$; otherwise, $m = 0$ and $n = 1$. For estimates in the important case where $ak_s z_p \lesssim 1$, the simple analytical approximation $F \simeq$

$1/[2\pi ak_s z_p]$ can be used (see figure). Note that the quantity $1/ak_s$ characterizes the penetration depth for SPPs into the dielectric.

Thus, in addition to the conditions $R_p \ll z_p$ and $R_p k_s \ll 1$, we obtain conditions (13)–(16), under which the electric field inside the scatterer may be treated as almost uniform. Note that the magnetic field in the scatterer is disregarded in this approximation from the very beginning. The substitution of the total electric field from Eq. (8), where only quasi-static terms are retained, into the expression for the electric dipole moment yields the known representation for the polarizability tensor $\hat{\alpha}_d$ of the spherical particle that is situated near the planar interface between two media:

$$\hat{\alpha}_d = \alpha_0\left(\hat{\mathbf{I}} - k_0^2\frac{\alpha_0}{\varepsilon_0}\hat{G}_q^s(\mathbf{r}_p, \mathbf{r}_p)\right)^{-1}. \quad (18)$$

Conditions (13)–(16) can be significantly simplified for the case where the role of the metal–dielectric interface in the determination of the scatterer polarizability is negligible, so that

$$\left|\frac{(1+a^2)(\varepsilon_p - \varepsilon_d)}{4(1-a^2)(\varepsilon_p + 2\varepsilon_d)}\left(\frac{R_p}{z_p}\right)^3\right| \ll 1. \quad (19)$$

In this case, conditions (13)–(16) reduce to the two inequalities

$$(k_d R_p)^2\left|\frac{\varepsilon_p - \varepsilon_d}{\varepsilon_p + 2\varepsilon_d}\right| \ll 1, \quad (20)$$

$$3k_0^3 V_p\left|\frac{\varepsilon_p - \varepsilon_d}{\varepsilon_p + 2\varepsilon_d}\right|\frac{a\varepsilon_d^{3/2}F(ak_s z_p)}{(1-a^2)^{3/2}(1-a^4)} \ll 1. \quad (21)$$

Note that the condition $R_p \ll z_p$ is not necessary in this case.

In experiments on the scattering of SPPs, the scatterer is often made of the same metal (e.g., gold or silver) as the substrate with SPPs ($\varepsilon_p = \varepsilon_m$). In this case, the dielectric over the substrate is air ($\varepsilon_d = 1$). In conclusion, for such material systems we estimate the scatterer radius R_p that satisfies the requirements of the dipole approximation. Let the wavelength of light exciting SPPs be equal to 800 nm. In this case, the imaginary part of the dielectric constant of gold is much smaller than the absolute value of the real part. For this reason, this imaginary part can be ignored, and we set $\varepsilon_m = \varepsilon_p \approx -26$ [14]. Note that the condition $R_p \ll z_p$ may be replaced by condition (19). Let us assume that z_p = 50 nm. In this case, the dominant conditions are inequalities (19) and (21), from which we obtain $R_p \ll$ 74 nm and $R_p \ll$ 71 nm, respectively. As the distance between the scatterer and surface with SPPs increases, the determining conditions become $R_p \ll 1/k_s$ and Eq. (20) ($R_p \ll$ 120 nm for z_p = 200 nm). Since the dielectric constant of silver at the given wavelength differs only slightly from the dielectric constant of gold, the resulting constraints on R_p are also valid for silver.

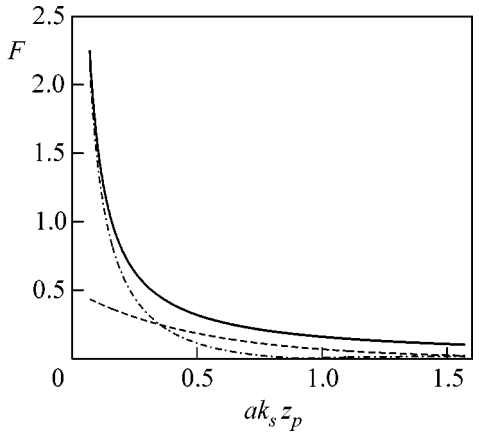

(Dashed line) The first and (dash–dotted line) second terms in Eq. (17) determining the function $F(ak_s z_p)$ and (solid line) the approximation for this function at $ak_s z_p \lesssim 1$.

REFERENCES

1. *Surface Polaritons*, Ed. by V. M. Agranovich and D. L. Mills (North-Holland, Amsterdam, 1982; Nauka, Moscow, 1985).
2. W. L. Barnes, A. Dereux, and T. W. Ebbesen, Nature **424**, 824 (2003).
3. A. V. Shchegrov, I. V. Novikov, and A. A. Maradudin, Phys. Rev. Lett. **78**, 4269 (1997).
4. S. I. Bozhevolnyi and V. Coello, Phys. Rev. B **58**, 10899 (1998).
5. S. Bozhevolnyi and V. Volkov, Opt. Commun. **198**, 241 (2001).
6. T. Søndergaard and S. I. Bozhevolnyi, Phys. Rev. B **67**, 165405 (2003).
7. V. Coello, T. Søndergaard, and S. I. Bozhevolnyi, Opt. Commun. **240**, 345 (2004).
8. V. I. Dmitriev and E. V. Zakharov, *Integral Equations in Boundary Value Problems of Electrodynamics* (Mosk. Gos. Univ., Moscow, 1987) [in Russian].
9. T. Søndergaard and S. I. Bozhevolnyi, Phys. Rev. B **69**, 045422 (2004).
10. L. D. Landau and E. M. Lifshitz, *Course of Theoretical Physics*, Vol. 8: *Electrodynamics of Continuous Media*, 3rd ed. (Nauka, Moscow, 1992; Pergamon, New York, 1984).
11. A. B. Evlyukhin and E. V. Evlyukhina, Opt. Zh. **71** (6), 58 (2004) [J. Opt. Technol. **71**, 384 (2004)].
12. O. Keller, Phys. Rep. **268**, 85 (1996).
13. O. Keller, J. Opt. Soc. Am. B **16**, 835 (1999).
14. E. Palik, *Handbook of Optical Constant of Solids* (Academic, San Diego, CA, 1985).

Translated by R. Tyapaev

JETP Letters, Vol. 81, No. 5, 2005, pp. 222–225. From Pis'ma v Zhurnal Éksperimental'noĭ i Teoreticheskoĭ Fiziki, Vol. 81, No. 5, 2005, pp. 283–286.

Dissymmetrical Tunneling in Heavy-Fermion Metals¶

V. R. Shaginyan

St. Petersburg Nuclear Physics Institute, Russian Academy of Sciences, Gatchina, 188300 Russia
CTSPS, Clark Atlanta University, Atlanta, Georgia 30314, USA
e-mail: vrshag@thd.pnpi.spb.ru

Received January 27, 2005

A tunneling conductivity between a heavy-fermion metal and a simple metallic point is considered. We show that, at low temperatures, this conductivity can be noticeably dissymmetrical with respect to the change of voltage bias. The dissymmetry can be observed in experiments on heavy-fermion metals whose electronic system has undergone the fermion-condensation quantum phase transition. © *2005 Pleiades Publishing, Inc.*

PACS numbers: 71.10.Hf, 71.27.+a, 75.30.Cr

Understanding the unusual quantum critical properties of heavy-fermion (HF) metals at low temperatures T remains challenging. It is a common belief that quantum phase transitions developing in HF metals at $T = 0$, which have the ability to influence the finite-temperature properties, are responsible for the anomalous behavior. Experiments on HF metals explore mainly their thermodynamic properties, which have proved to be quite different from those of ordinary metals described by the Landau Fermi liquid (LFL) theory. In the LFL theory, considered to be the main instrument of investigating quantum many-electron physics, the effective mass M^* of quasiparticle excitations controlling the density of states determines the thermodynamic properties of electronic systems. It is possible to explain the observed thermodynamic properties of HF metals on the basis of the fermion-condensation quantum phase transition (FCQPT), which allows the existence of the Landau quasiparticles down to the lowest temperatures [1, 2]. In contrast to the Landau quasiparticles, these are characterized by an effective mass that strongly depends on the temperature T, applied magnetic field B, and number density x of the heavy-electron liquid of the HF metal. Thus, we return again to the key role of the density of state. It would be desirable to probe the other properties of the heavy-electron liquid, such as the probabilities of quasiparticle occupations, which are not directly linked to the density of states or to the behavior of M^*. Scanning tunneling microscopy, which is sensitive to both the density of states and to the probabilities of quasiparticle occupations, is an ideal technique for the study of such effects at the quantum level.

The tunneling current I through a point contact between two ordinary metals is proportional to the driving voltage V and to the squared modulus of the quantum–mechanical transition amplitude t multiplied by the difference $N_1(0)N_2(0)(n_1(p, T) - n_2(p, T))$ (see, e.g., [3]). Here, $n(p, T)$ is the quasiparticle distribution function and $N(0)$ is the density of states of the corresponding metal. On the other hand, the wavefunction calculated in the WKB approximation and defining t is proportional to $(N_1(0)N_2(0))^{-1/2}$. As a result, the density of states is dropped out, and the tunneling current does not depend on $N_1(0)N_2(0)$. Upon taking into account that, at $T \longrightarrow 0$, the distribution $n(p, T \longrightarrow 0) \longrightarrow n_F(p)$, where $n_F(p)$ is the step function $\theta(p - p_F)$ with p_F being the Fermi momentum, one can check that, within the LFL theory, the differential tunneling conductivity $\sigma_d(V) = dI/dV$ is a symmetric function of the voltage V. In fact, the symmetry of $\sigma_d(V)$ holds provided that so-called particle–hole symmetry is preserved, as it is within the LFL theory, but the relation $n(p, T \longrightarrow 0) \longrightarrow \theta(p - p_F)$ will do. Therefore, the existence of the $\sigma_d(V)$ symmetry is quite obvious and common in the case of metal-to-metal contacts when these metals are in the normal state or in the superconducting one.

In this letter, we show that the situation can be different when one of the two metals is a HF metal whose electronic system is represented by the heavy-electron liquid. When the heavy-electron liquid has undergone FCQPT, its distribution function is no longer the step function as soon as the temperature tends to zero [4]. As a result, both the differential tunneling conductivity $\sigma_d(V)$ and the tunneling conductivity $\sigma(V)$ become dissymmetrical as a function of voltage V, though the application of a magnetic field destroying the non-Fermi-liquid behavior of the heavy-electron liquid restores the symmetry.

At first, we briefly describe the heavy-electron liquid with the fermion condensate (FC) [4–6]. When the number density x of the liquid approaches some density x_{FC}, the effective mass diverges. Because the kinetic energy near the Fermi surface is proportional to the inverse effective mass, FCQPT is triggered by the frus-

¶ This article was submitted by the author in English.

trated kinetic energy. Behind the critical point x_{FC}, the quasiparticle distribution function represented by $n_F(p)$ does not deliver the minimum of the Landau functional $E[n(\mathbf{p})]$. As a result, at $x < x_{FC}$, the quasiparticle distribution is determined by the standard equation to search for the minimum of a functional [4]:

$$\frac{\delta E[n(\mathbf{p})]}{\delta n(\mathbf{p}, T=0)} = \varepsilon(\mathbf{p}) = \mu; \quad p_i \le p \le p_f. \tag{1}$$

Equation (1) determines the quasiparticle distribution function $n_0(\mathbf{p})$ that delivers the minimum value of the ground-state energy E. Determined by Eq. (1), the function $n_0(\mathbf{p})$ does not coincide with the step function $n_F(p)$ in the region $(p_f - p_i)$, so that $0 < n_0(\mathbf{p}) < 1$; however, outside the region, it coincides with $n_F(p)$. It follows from Eq. (1) that the single-particle spectrum is completely flat over the region. Such a state was called the state with a FC, because quasiparticles located in the region $(p_f - p_i)$ of momentum space are pinned to the chemical potential μ. We note that the behavior obtained was observed within exactly solvable models [7, 8] and represents a new state of Fermi liquid [9]. We can conclude that the relevant order parameter $\kappa(\mathbf{p}) = \sqrt{n_0(\mathbf{p})(1-n_0(\mathbf{p}))}$ is the order parameter of the superconducting state with an infinitely small value of the superconducting gap Δ [5]. Thus, this state cannot exist at any finite temperatures and is driven by the parameter x: at $x > x_{FC}$, the system is on the disordered side of FCQPT; at $x = x_{FC}$, Eq. (1) possesses the nontrivial solutions $n_0(\mathbf{p})$ with $p_i = p_F = p_f$; at $x < x_{FC}$, the system is on the ordered side. At $T > 0$, the quasiparticle distribution is given by

$$n(\mathbf{p}, T) = \left\{1 + \exp\left[\frac{(\varepsilon(\mathbf{p}, T) - \mu)}{T}\right]\right\}^{-1}, \tag{2}$$

where $\varepsilon(\mathbf{p}, T)$ is the single-particle spectrum, or dispersion, of the quasiparticle excitations and μ is the chemical potential. Equation (2) can be recast as

$$\varepsilon(\mathbf{p}, T) - \mu(T) = T\ln\frac{1 - n(\mathbf{p}, T)}{n(\mathbf{p}, T)}. \tag{3}$$

As $T \longrightarrow 0$, the logarithm on the right-hand side of Eq. (3) is finite when p belongs to the regions $(p_f - p_i)$; therefore, $T\ln(\ldots) \longrightarrow 0$, and we again arrive at Eq. (1). Near the Fermi level, the single-particle spectrum can be approximated as

$$\varepsilon(p \simeq p_F, T) - \mu \simeq \frac{p_F(p - p_F)}{M^*}. \tag{4}$$

It follows from Eq. (2) that $n(p, T \longrightarrow 0) \longrightarrow n_F(p)$ provided that M^* is finite at $T \longrightarrow 0$. Thus, at low temperatures, the left-hand side of Eq. (3) determines the behavior of the right-hand side. In contrast to this case, the right-hand side of Eq. (3) determines the behavior of M^* when a FC is set for the liquid. Indeed, it follows from Eq. (1) that $n(\mathbf{p}, T \longrightarrow 0) = n_0(\mathbf{p})$. Therefore, at low temperatures, as seen from Eq. (3), the effective mass diverges as [10]

$$M^*(T) \simeq p_F\frac{p_f - p_i}{4T}. \tag{5}$$

At $T \ll T_f$, Eq. (5) is valid and determines quasiparticles with the energy z and characterized by the distribution function $n_0(p)$. Here, T_f is the temperature at which the influence of FCQPT vanishes [5]. The energy z belongs to the interval

$$\mu - 2T \le z \le \mu + 2T. \tag{6}$$

Now, we turn to a consideration of the tunneling current at low temperatures, which, in the case of ordinary metals, is given by [3]

$$I(V) = 2|t|^2\int[n_F(z-\mu) - n_F(z-\mu+V)]dz. \tag{7}$$

We use an atomic system of units: $e = m = \hbar = 1$, where e and m are electron charge and mass, respectively. Since temperatures are low, we approximate the distribution function of an ordinary metal by the step function n_F. It follows from Eq. (7) that quasiparticles with the energy z, $\mu - V \le z \le \mu$, contribute to the current, while $\sigma_d(V) \simeq 2|t|^2$ is a symmetrical function of V. In the case of the heavy-electron liquid with a FC, the tunneling current is found to be of the form

$$I(V) = 2\int[n_0(z-\mu) - n_F(z-\mu+V)]dz. \tag{8}$$

Here, we have replaced the distribution function of an ordinary metal with n_0, the solution of Eq. (1). We have also taken units such that $|t|^2 = 1$. Assume that V satisfies the condition $|V| \le 2T$, while the current flows from the HF metal to the ordinary one. Quasiparticles of energy z, $\mu - V \le z$, contribute to $I(V)$, and the differential conductivity $\sigma_d(V) \simeq 2n_0(z \simeq \mu - V)$. If the sign of the voltage is changed, the direction of the current is also changed. In that case, quasiparticles of the energy z, $\mu + V \ge z$, contribute to $I(V)$, and the differential conductivity $\sigma_d(-V) \simeq 2(1 - n_0(z \simeq \mu + V))$. The dissymmetrical part $\Delta\sigma_d(V) = (\sigma_d(-V) - \sigma_d(V))$ of the differential conductivity is of the form

$$\Delta\sigma_d(V) \simeq 2[1 - (n_0(z-\mu \simeq V) + n_0(z-\mu \simeq -V))]. \tag{9}$$

It is worth noting that it follows from Eq. (9) that $\Delta\sigma_d(V) = 0$ if the HF metal in question is replaced by an ordinary metal. Indeed, if the effective mass is finite at $T \longrightarrow 0$, then $n_0(T \longrightarrow 0) \longrightarrow n_F$ is given by Eq. (2) and $1 - n(z - \mu \simeq V) = n(z - \mu \simeq -V)$. One might say that the dissymmetrical part vanishes due to the particle–hole symmetry. On the other hand, there are no reasons to expect that $(1 - n_0(z - \mu \simeq V) - n_0(z - \mu \simeq -V)) = 0$. Thus, we are led to the conclusion that the differential conductivity becomes a dissymmetrical function of the voltage. To estimate $\Delta\sigma_d(V)$, we observe that this is zero when $V = 0$, because $n_0(p = p_F) = 1/2$ as it should be, and

it follows from Eq. (3) as well. It is seen from Eq. (9) that $\Delta\sigma_d(V)$ is an even function of V. Therefore, we can assume that, at low values of the voltage V, the dissymmetrical part behaves as $\Delta\sigma_d(V) \propto V^2$. Then, the natural scale to measure the voltage is $2T$, as is seen from Eq. (6). In fact, the dissymmetrical part should be proportional to $(p_f - p_i)/p_F$. As a result, we obtain

$$\Delta\sigma_d(V) \simeq c\left(\frac{V}{2T}\right)^2 \frac{p_f - p_i}{p_F}. \quad (10)$$

Here, c is a constant, which is expected to be of the order of unity. This constant can be evaluated using analytical solvable models. For example, calculations of c within a simple model, when the Landau functional $E[n(p)]$ is of the form [4]

$$E[n(p)] = \int \frac{p^2}{2M}\frac{d\mathbf{p}}{(2\pi)^3} + V_1\int n(p)n(p)\frac{d\mathbf{p}}{(2\pi)^3}, \quad (11)$$

give that $c \simeq 1/2$. It follows from Eq. (10) that, when $V \simeq 2T$ and a FC occupies a noticeable part of the Fermi volume, $(p_f - p_i)/p_F \simeq 1$, the dissymmetrical part becomes comparable with differential tunneling conductivity, $\Delta\sigma_d(V) \sim V_d(V)$.

The dissymmetrical behavior of the tunneling conductivity can be observed in measurements of heavy-fermion metals such as, for example, $YbRh_2(Si_{0.95}Ge_{0.05})_2$ or $YbRh_2Si_2$, which are expected to have undergone FCQPT. In that case, upon the application of a magnetic field B, the effective mass should diverge as [1, 11]

$$M^*(B) \propto (B - B_{c0})^{\alpha}. \quad (12)$$

Here, B_{c0} is the critical magnetic field that drives the HF metal to its magnetic-field-tuned quantum critical point. The value of the critical exponent $\alpha = -1/2$ is in good agreement with experimental observations collected of these metals [12, 13]. The measurements of $\Delta\sigma_d(V)$ have to be carried out while applying a magnetic field B_{c0} at temperatures $T \le T_f$. In the case of these metals, T_f is of the order of a few kelvin [11]. We note that, at sufficiently low temperatures, the application of a magnetic field $B > B_{c0}$ leads to the restoration of the Landau Fermi liquid with $M^*(B)$ given by Eq. (12) [1, 11]. As a result, the dissymmetrical behavior of the tunneling conductivity vanishes.

The dissymmetrical differential conductivity $\Delta\sigma_d(V)$ can also be observed when the HF metal in question goes from normal to superconducting. The reason is that $n_0(p)$ is again responsible for the dissymmetrical part of $\sigma_d(V)$. This $n_0(p)$ is not appreciably disturbed by the pairing interaction, which is relatively weak as compared to the Landau interaction forming the distribution function $n_0(p)$ [10, 14]. In the case of superconductivity, we have to take into account that the density of states,

$$\frac{N_s(E)}{N(0)} = \frac{|E|}{\sqrt{E^2 - \Delta^2}}, \quad (13)$$

comes into the play because N_s is zero in the gap, that is, when $|E| \le |\Delta|$. Here, E is the quasiparticle energy, while the normal state quasiparticle energy is $\varepsilon - \mu = \sqrt{E^2 - \Delta^2}$. Now, we can arrange Eq. (9) for the case of a superconducting HF metal by multiplying the right-hand side of Eq. (9) by $N_s/N(0)$ and replacing the quasiparticle energy $z - \mu$ by $\sqrt{E^2 - \Delta^2}$, with E being represented by the voltage V. As a result, Eq. (10) can be cast into the following form:

$$\Delta\sigma_d(V) \simeq \frac{(\sqrt{V^2 - \Delta^2})^2}{|\Delta|\sqrt{V^2 - \Delta^2}}\frac{p_f - p_i}{p_F} = \sqrt{\left[\frac{V}{\Delta}\right]^2 - 1}\frac{p_f - p_i}{p_F}. \quad (14)$$

Note that the scale $2T$ entering into Eq. (10) is replaced by the scale Δ in Eq. (14). In the same way, as Eq. (10) is valid up to $V \simeq 2T$, Eq. (14) is valid up to $V \simeq 2|\Delta|$. It is seen from Eq. (14) that the dissymmetrical part of the differential tunneling conductivity becomes as large as the differential tunneling conductivity at $V \simeq 2|\Delta|$ provided that a FC occupies a large part of the Fermi volume, $(p_f - p_i)/p_F \simeq 1$. In the case of a d-wave gap, the right-hand side of Eq. (14) has to be integrated over the gap distribution. As a result, $\Delta\sigma_d(V)$ is expected to be finite even at $V = \Delta_1$, where Δ_1 is the maximum value of the d-wave gap. A detailed consideration of the superconducting case will be published elsewhere.

In summary, we have shown that the differential tunneling conductivity between a metallic point and an ordinary metal, which is commonly symmetric as a function of the voltage, becomes noticeably dissymmetrical when the ordinary metal is replaced by a HF metal, the electronic system of which has undergone FCQPT. This dissymmetry can be observed when the HF metal is both normal and superconducting. We have also discussed possible experiments to study the dissymmetry.

I am grateful to Dr. A.Z. Msezane for the kind hospitality at CTSPS, Clark Atlanta University, Atlanta, GA, USA, where part of this work was done.

REFERENCES

1. V. R. Shaginyan, JETP Lett. **79**, 286 (2004).
2. J. W. Clark, V. A. Khodel, and M. V. Zverev, Phys. Rev. B **71**, 012 401 (2005).
3. A. M. Zagoskin, *Quantum Theory of Many-Body Systems* (Springer, New York, 1998).

4. V. A. Khodel and V. R. Shaginyan, JETP Lett. **51**, 553 (1990).
5. V. A. Khodel, V. R. Shaginyan, and V. V. Khodel, Phys. Rep. **249**, 1 (1994); V. A. Khodel and V. R. Shaginyan, Condens. Matter Theor. **12**, 222 (1997); J. Dukelsky *et al.*, Z. Phys. B **102**, 245 (1997).
6. V. R. Shaginyan, JETP Lett. **77**, 99 (2003); JETP Lett. **77**, 178 (2003).
7. V. Yu. Irkhin, A. A. Katanin, and M. I. Katsnelson, Phys. Rev. Lett. **89**, 076401 (2002).
8. D. Lidsky, J. Shiraishi, Y. Hatsugai, and M. Kohmoto, Phys. Rev. B **57**, 1340 (1998).
9. G. E. Volovik, JETP Lett. **53**, 222 (1991).
10. M. Ya. Amusia and V. R. Shaginyan, Phys. Rev. B **63**, 224507 (2001).
11. Yu. G. Pogorelov and V. R. Shaginyan, JETP Lett. **76**, 532 (2002); V. R. Shaginyan, A. Z. Msezane, and M. Ya. Amusia, cond-mat/0501093.
12. P. Gegenwart *et al.*, Phys. Rev. Lett. **89**, 056402 (2002).
13. J. Custers *et al.*, Nature **424**, 524 (2003).
14. M. Ya. Amusia, S. A. Artamonov, and V. R. Shaginyan, JETP Lett. **74**, 396 (2001).

JETP Letters, Vol. 81, No. 5, 2005, pp. 226–230. Translated from Pis'ma v Zhurnal Éksperimental'noĭ i Teoreticheskoĭ Fiziki, Vol. 81, No. 5, 2005, pp. 287–291.

Electron Transport in Monodisperse Metal Nanostructures

V. I. Kozub, V. M. Kozhevin, D. A. Yavsin, and S. A. Gurevich

Ioffe Physicotechnical Institute, Russian Academy of Sciences, St. Petersburg, 194021 Russia

e-mail: Ven.Kozub@mail.ioffe.ru

Received February 3, 2005

Electron transport in monodisperse granular Cu, Ni, and Pd structures with conduction near the percolation threshold is investigated. An activation conduction law is observed in the oxidized Cu structures, whereas the Efros–Shklovskii law is observed in the initial Cu structures and in the Ni and Pd structures. This behavior is discussed within the framework of a model in which variable range hopping conduction is considered with regard to both the disorder potential and spread of the sizes of grain assemblies. © *2005 Pleiades Publishing, Inc.*

PACS numbers: 73.63.–b, 81.07.–b

Metal nanostructures are, with increasing frequency, being considered key elements of various technologies, for example, in the development of new nanoelectronic devices [1] or highly efficient catalysts [2]. The prospects for the applications of such structures are determined by their unusual electric properties, which depend on factors of structure and energy disorder (such as the spread of particle sizes, the character of correlations in the mutual arrangement of these particles, or the value of the random potential). However, possibilities for experimental studies that would provide detailed information on physical phenomena in the indicated structures have been restricted until recently, because the effects of these factors are manifested simultaneously in real nanostructures formed using conventional procedures. At the same time, the physical nature of electron transport in granular structures is far from being completely understood in the theoretical aspect as well. Here, the difficulty of simultaneously taking into account various kinds of disordering is also important. However, in recent years, new technologies have emerged that allow for the creation of nanostructures in which the effect of some factors of disorder can be neglected. Studying such structures allows one to verify the applicability of various theoretical models to the description of transport processes. This work is devoted to the study of granular metal (Cu, Ni, and Pd) films obtained by one of the new technologies, namely, laser electrodispersion [3]. The most important feature of this technique is that the resulting structures consist of spherical metal nanoparticles with relative size dispersion <0.1, so that the nanostructures under study may be considered as monodisperse. In addition, the mean size of nanoparticles is determined only by the properties of the material from which these particles are manufactured. Thus, the diameter of nanoparticles equals 5 nm for Cu, 2.5 nm for Ni, and 2 nm for Pd. Depending on the film deposition time, the density of particles on the substrate surface can vary in the range from one partially filled layer of particles to several close-packed layers of particles. The prepared films were kept in air and were thereby partially oxidized. It is important to note that the structural features of films, such as the character of the mutual arrangement of nanoparticles or the thickness of their oxide shell, are also determined primarily by the material of the particles.

We compare the structure of Cu, Ni, and Pd films where the density of particles is such that conduction in these films is due to tunnel electron transport (below the percolation threshold). For Cu films, this kind of conduction is provided when the surface density of particles is 0.9 M, where M is the density of one completely filled layer. A microphotograph of such a film is shown in Fig. 1a. The figure demonstrates that the structure of the film is inhomogeneous: particles form assemblies composed of several closely adjoining grains. An analysis of the image shows that the assemblies consist of 1–15 particles, and the probability P_V of finding an assembly with volume V is given by the expression $P_V = A/V$. The constant A is found from the normalization condition $A = (\ln V_{max}/V_{min})^{-1}$. These assemblies are separated by a network of dielectric gaps whose width exceeds 3 nm. Because tunneling through such a gap is highly improbable, a current in the structure can flow only because of tunneling through a small number of particles connecting the assemblies.

A microphotograph of a Ni film is shown in Fig. 1b. It is seen that the distribution of Ni nanoparticles over the substrate surface is also nonuniform; however, most particles are grouped into assemblies that mainly have the form of chains. As in the case of Cu structures, the distribution of assembly sizes obeys the law $P_V = A/V$. Note that the structure of Pd films is similar to the structure of Ni films and that both structures exhibit conduction properties starting with the instant when the first layer of particles is filled by more than a quarter, that is,

0021-3640/05/8105-0226$26.00 © 2005 Pleiades Publishing, Inc.

at a mean density of particles of 0.25 M. The sizes of gaps between assemblies in such structures are less than 2 nm, and electron tunneling between isolated assemblies is quite feasible.

Measurements have shown that the oxidation of Cu films substantially affects their electric properties. Figure 2 demonstrates temperature dependences of the conductivity of the same film, one of which was measured immediately after preparation and the other of which was measured after the film was exposed to air for a week. It is evident that the fully oxidized film demonstrates an activation dependence of the conductivity that linear on the coordinates ($\ln\sigma$, $1/T$). At the same time, the temperature dependence of the conductivity of the freshly prepared film is significantly weaker.

We believe that this difference is due to the effect of the process of oxidation of Cu nanoparticles on the film structure. At small oxidation times (1–2 days), the metal particles are not oxidized and, contacting each other, form conducting assemblies. After oxidation for 10 days or longer, all the Cu nanoparticles are covered with a Cu_2O layer 0.7–0.8 nm thick (correspondingly, the diameter of the remaining metal core equals $\simeq$3.5 nm), after which oxidation terminates [4]. In such strongly oxidized structures, metal cores are separated from each other by a nonconducting layer even at tight contact; that is, during oxidation, conducting assemblies are divided into separate particles.

Nickel and palladium particles are of lower oxidative capacity than Cu ones; therefore, oxidation slightly affected the conductivities of the structures of these metals. Figure 3 presents the temperature dependences of the conductivity of Pd and Ni nanostructures measured after the exposure of films to air for several weeks. It is evident in the figure that these dependences are similar to the temperature dependences of the conductivity of partially oxidized Cu nanostructures and are linear in the coordinates ($\ln\sigma$, $(1/T)^{1/2}$).

Thus, nanostructures composed of monodisperse spherical metal grains, for which an activation dependence of the conductivity was expected to be natural, exhibit such a dependence only in the case of oxidized Cu films. In all other cases, the temperature dependence of the film conductivity is close to $\exp(-(T_0/T)^{-1/2})$.

While the activation dependence of the conductivity observed in granular structures is readily explained by the Coulomb blockade effects, the dependence $\exp(-(T_0/T)^{1/2})$ has been a subject of discussion for many years. From the arguments by Efros and Shklovskii [5], it is clear that this behavior is connected with the role of disorder. It was suggested in [6] that disorder is associated with the spread of particle sizes and the Efros–Shklovskii (ES) law is fulfilled due to correlation between the size of particles and the distance between them. It is unlikely, however, that this correlation is universal for structures obtained using various technologies. Some other mechanisms were also discussed, in particular, the discreteness of particle energy levels [7], disorder in the arrangement of impurities [8], and fluctuations associated with the surface energy [9]. However, the above mechanisms are not important for the structures investigated in our work, which consist of quite large particles.

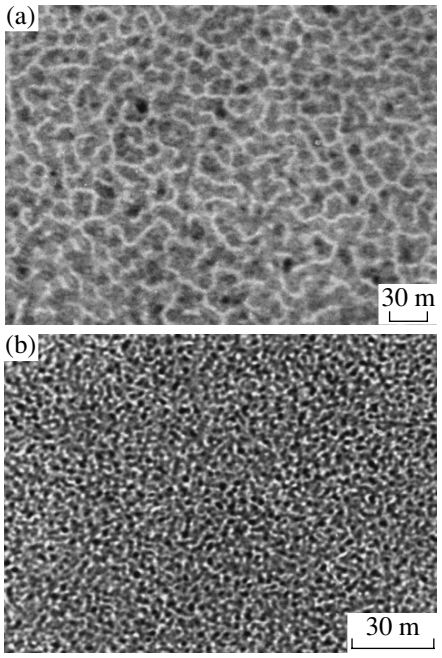

Fig. 1. Microphotographs obtained by transmission electron microscopy for (a) copper film (sputtering time 5 min) and (b) nickel film (sputtering time 15 s).

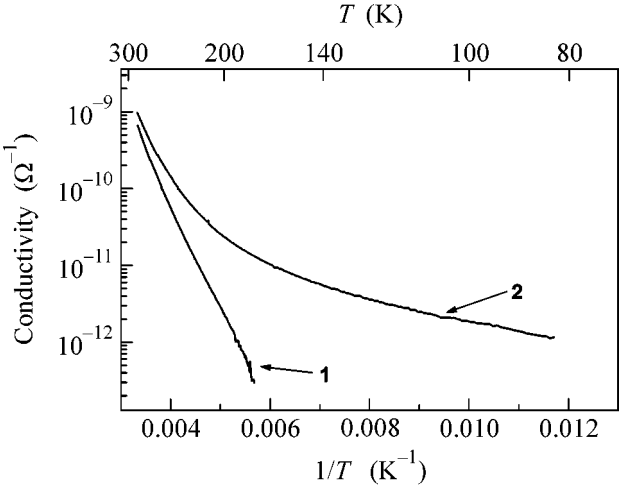

Fig. 2. Temperature dependences of the conductivity of the (*1*) oxidized and (*2*) freshly prepared Cu film.

All the approaches mentioned above considered electron hops between neighboring particles. Only in a

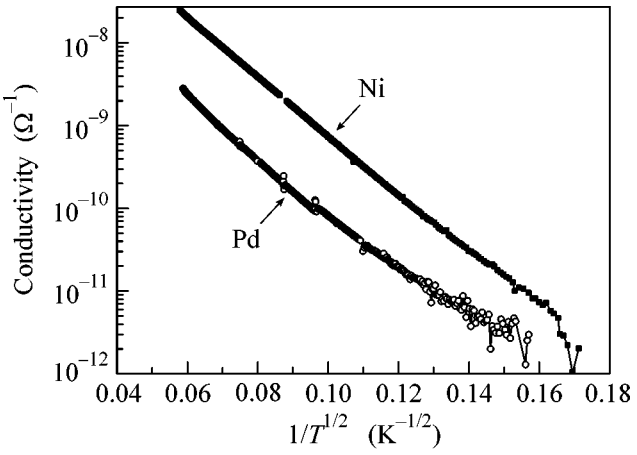

Fig. 3. Temperature dependences of the conductivity of Ni and Pd films.

recent work [10] has an explanation of the ES law been suggested based on the consideration of a combination of the disorder potential (associated with background traps) with the possibility of hops between distant particles, when the tunneling electron crosses a number of intermediate particles. In this case, hops between distant particles have been considered in the framework of semiqualitative estimates. In our opinion, the possibility of hops between distant particles involving intermediate particles is decisive for the explanation of the ES law for granular systems.

We will analyze two possible situations. The first one suggests the dominating effect of the disorder potential associated, e.g., with charged traps in dielectric interlayers. Its analysis will be based on the same arguments as were presented in [10]. In the other situation, energy disorder is associated with the self-organization of particles into assemblies whose sizes exhibit a significant spread.

Before beginning a detailed analysis, we note that the comparison of the problem of electron transport in granular materials with the problem of hopping conduction in semiconductors provides for the conclusion that the Coulomb blockade effect is analogous to the on-site electron–electron repulsion and that transport under the Coulomb blockade conditions is analogous to transport over the upper Hubbard band. If the Fermi level position is the same in different particles, transport under the Coulomb blockade conditions is associated with the activation of electrons from the Fermi level to the upper Hubbard band. In this case, the conductivity obeys an activation law, and the activation energy is the Coulomb blockade energy $E_C = e^2/C$, where C is the particle capacitance in the structure.

In the presence of a fluctuating potential, the electron energy in the particle is

$$\varepsilon_{\mathbf{p}} + U,$$

where $\varepsilon_{\mathbf{p}}$ is the kinetic energy and U is the local value of the particle potential. The values of U are different for different particles and have a spread ΔU. As a result, the Fermi level positions μ with respect to vacuum for conduction electrons are different for different particles. It might be expected that electron exchange between individual particles should maintain a common level of the chemical potential on the same pattern. However, the Coulomb blockade effects prevent this kind of leveling, so that the spread of the Fermi levels in particles is retained in the system. If $\Delta U > E_C$, the scale of the spread is determined by the energy E_C.

Because electron transfer proceeds over states in the vicinity of the Fermi level, the change in energy upon electron transfer between two particles is

$$\mu_1 - \mu_2 + E_C - \frac{e^2}{C_{12}}, \tag{1}$$

where C_{12} is the mutual capacitance of the particles. It is evident that, because of the spread of μ, the electron transfer activation energy can be reduced to zero. Note that the arguments presented are mainly analogous to those given in [10]. The situation is similar to hopping conduction in semiconductors in the case where the upper and lower Hubbard bands overlap due to the disorder energy. The latter term in Eq. (1) corresponds to the Coulomb interaction energy between the electron that is transferred from one particle to another and the remaining hole and leads to a Coulomb gap in the distribution of quasi-Fermi level positions in various particles. This gap is analogous to the Coulomb gap for the density of localized states in semiconductors.

Thus, at sufficiently high E_C and low temperatures, variable range hopping conduction can be manifested: the activation energy for transitions between distant particles can be lower than the energy required for transition between the neighboring particles. At a high particle density in the structure, which is characteristic of the case under consideration, hops between distant particles must occur through intermediate metal particles.

In order to describe such a hop, we will use an approach similar to that used by Shklovskii and Spivak [11] (see also [12]), in which hops are considered through intermediate sites. Let us estimate the probability of a hop between particles 1 and 3 through intermediate particle 2 within the framework of perturbation theory, taking into account the change in the electron states of individual particles due to tunneling to other particles. According to calculations similar to those made in [11, 12], the probability of such a hop is

$$\frac{1}{\tau_{\text{e-ph}}}\sum_{\varepsilon_{3,j}}\sum_{\varepsilon_{2,i}}\frac{I_{1,2}^2}{(\varepsilon_1-\varepsilon_{2,i})^2+I^2}\frac{I_{2,3}^2}{(\varepsilon_2-\varepsilon_{3,j})^2+I^2} \times \exp\left(-\frac{|\varepsilon_1-\varepsilon_{3,j}+E_C|}{T}\right). \tag{2}$$

Here, τ_{e-ph} is the electron–phonon relaxation time in the particles, $I_{m,n}$ are overlap integrals between electron states of the corresponding particles, I is the width of energy states in the particles, and the summations are carried out over all available states of particles 2 and 3. The summation with respect to $\varepsilon_{2,i}$ is performed over strips of width I in the vicinity of energies ε_1 and $\varepsilon_{3,j}$. The summation with respect to $\varepsilon_{3,j}$ is carried out over a strip of width $\sim T$ in the vicinity of the Fermi level of particle 3.

The most important fact is that the tunneling exponent is determined by a simple sum of exponents describing tunneling of particle 1 to particle 2 and particle 2 to particle 3 (entering into expressions for the overlap integrals $I_{1,2}$ and $I_{2,3}$), whereas the parameters of intermediate grain 2 enter only into the preexponential factor.

Analogous considerations can also be used to describe a hop over a greater number of intermediate particles (cf. [11]), which substantiates the concept of variable range hopping conduction for granular systems. The tunneling exponent for a hop over a distance r is estimated at $\sim d_i(r/ad_g)$, where d_i is the characteristic size of the dielectric gap between individual particles, d_g is the size of the metal core of the particle, and a is the electron localization length in the insulated interlayer. It is clear that the effective localization length for a hop over intermediate particles is $a_{\text{eff}} \sim ad_g/d_i$.

For hops with an energy deficit less than E_C, the existence of a Coulomb gap in the distribution of particle Fermi levels is important: it leads to the ES law for the conductivity $\sigma \propto \exp -(T_0/T)^{1/2}$, where $T_0 = e^2/\kappa_{\text{eff}}a_{\text{eff}}$. The dielectric constant κ_{eff} is determined by screening processes in the structure. (Note that the presented expression is similar to that given in [10], where κ_{eff} was estimated at $\kappa d_g/d_i$.)

Let us now suppose that the disorder potential is absent and consider a nanostructure composed of close-packed assemblies of particles in which the spread of assembly sizes corresponds to the experimentally observed distribution $P_V = A/V$. Because $P_V \propto (1/r_V)^d$ and $V \propto C_V^d$ (where d is the dimension of the structure, C_V is the capacitance of the grain assembly of volume V, and r_V is the mean distance between the centers of such assemblies), it is evident that $r_V \propto C_V$. Hence, the Coulomb blockade energy for grain assemblies of a given volume depends on the distance between grains as $U_{C,V} = e^2A^{1/d}/\kappa_{\text{eff}}r_V$, and the probability of a hop between them is

$$p \propto \exp\left(-\left(\frac{2r_V}{a_{\text{eff}}} + \frac{e^2A}{\kappa_{\text{eff}}r_VT}\right)\right).$$

The optimization of the exponent with respect to r_V leads to the law $(T_0/T)^{-1/2}$, where T_0 differs from the estimate obtained for the disorder potential model by a factor of $\ln^{-1/d}(V_{\max}/V_{\min}) < 1$. It is unlikely that this factor can strongly differ from unity. Therefore, a choice in favor of a certain model must based not only on an analysis of the slopes of the temperature dependences of the conductivity but also on additional information about the properties of the structures.

Let us now turn to the analysis of experimental data. The activation character of conduction in the fully oxidized Cu films points to the absence of energy disorder and a small effect of the random potential in such structures. The energy of a charged particle calculated from the slope of curve *1* in Fig. 2 equals 200 meV and corresponds to $d_g \sim 3.5$. Considering that the disorder potential must increase with the degree of oxidation and that the disorder effect is absent for the oxidized films, it is natural to attribute the nonlinear temperature dependence of the conductivity for freshly prepared Cu films (curve *2*) to the spread of the sizes of particle assemblies, which coincides with the results of structural investigations.

In contrast to the Cu structures, the Pd and Ni structures exhibit a pronounced ES law in a wide temperature range (in the decade limits). In this case, according to Fig. 3, the value of T_0 is estimated at ~0.1 eV, which corresponds to $d_g/d_i \sim 3$. This agrees with our inference that the gaps between individual assemblies of particles are less than the mean assembly size (see Fig. 1b). Thus, taking into account the character of the distribution of Pd and Ni particles over the surface, it may be expected that the spread of the sizes and shapes of the particle assemblies is responsible for the disorder of the system. Note that the explanation of the observed effect when the ES law is obeyed for a change in the temperature by a decade requires the existence of assemblies of 15–20 particles in size.

In summary, we investigated hopping electron transport in monodisperse granular Cu, Ni, and Pd films with conductivity below the percolation threshold. The possibility of the manifestation of both the activation behavior of the conductivity and the Efros–Shklovskii law in such structures is associated with the presence of conducting assemblies composed of 1–15 particles. It is shown that, for the explanation of experimental results, it is necessary to invoke a model in which variable range hopping conduction via intermediate particles is considered.

This work was supported by the Russian Foundation for Basic Research (project nos. 03-02-17516a and 03-02-17638), the International Science and Technology Center (project no. B-678), the Federal Science and Technology Program "Physics of Solid-State Nanostructures," the Presidium of the Branch of General Physics and Astronomy, Russian Academy of Sciences (Program "New Materials"), and the Presidium of the Russian Academy of Sciences (program "Low-Dimensional Quantum Structures").

REFERENCES

1. R. H. Chen and K. K. Likharev, Appl. Phys. Lett. **72**, 61 (1998).
2. V. M. Kozhevin, D. A. Yavsin, S. A. Gurevich, *et al.*, in *Proceedings of 10th International Symposium on Nanostructures: Physics and Technology* (St. Petersburg, Russia, 2002), p. 41.
3. V. M. Kozhevin, D. A. Yavsin, S. A. Gurevich, *et al.*, J. Vac. Sci. Technol. B **18**, 1402 (2000).
4. V. M. Kozhevin, D. A. Yavsin, S. A. Gurevich, *et al.*, Fiz. Tverd. Tela (St. Petersburg) **45**, 1895 (2003) [Phys. Solid State **45**, 1993 (2003)].
5. B. I. Shklovskiĭ and A. L. Éfros, *Electronic Properties of Doped Semiconductors* (Nauka, Moscow, 1979; Springer, New York, 1984).
6. P. Sheng, B. Abeles, and Y. Arie, Phys. Rev. Lett. **31**, 44 (1973).
7. S. T. Chui, Phys. Rev. B **43**, 14 274 (1991).
8. E. Cuevas, M. Ortuno, and J. Ruiz, Phys. Rev. Lett. **71**, 1871 (1993).
9. E. M. Baskin and M. V. Entin, Pis'ma Zh. Éksp. Teor. Fiz. **70**, 510 (1999) [JETP Lett. **70**, 520 (1999)].
10. J. Zhang and B. I. Shklovskii, Phys. Rev. B **70**, 115317 (2004).
11. B. I. Shklovskii and B. Z. Spivak, in *Hopping Transport in Solids*, Ed. by M. Pollak and B. Shklovskii (Elsevier, Amsterdam, 1991), p. 271.
12. M. E. Raikh and G. F. Wessels, Phys. Rev. B **47**, 15609 (1993).

Translated by A. Bagatur'yants

JETP Letters, Vol. 81, No. 5, 2005, pp. 231–235. From Pis'ma v Zhurnal Éksperimental'noĭ i Teoreticheskoĭ Fiziki, Vol. 81, No. 5, 2005, pp. 292–296.

Pure Spin Photocurrents in Low-Dimensional Structures¶

S. A. Tarasenko and E. L. Ivchenko

Ioffe Physicotechnical Institute, Russian Academy of Sciences, St. Petersburg, 194021 Russia
e-mail: tarasenko@coherent.ioffe.ru

Received February 8, 2005

As is well known, the absorption of circularly polarized light in semiconductors results in optical orientation of electron spins and helicity-dependent electric photocurrent, and the absorption of linearly polarized light is accompanied by optical alignment of electron momenta. Here, we show that the absorption of unpolarized light leads to the generation of a pure spin current, although both the average electron spin and electric current vanish. We demonstrate this for direct interband and intersubband as well as indirect intraband (Drude-like) optical transitions in semiconductor quantum wells. © *2005 Pleiades Publishing, Inc.*

PACS numbers: 72.25.–b, 73.63.Hs, 78.67.De

1. INTRODUCTION

Spin and charge are among the basic properties of elementary particles such as electrons, positrons, and protons. The perturbation of a system of electrons by an electric field or light may lead to a flow of the particles. The typical example is an electric current, which represents the directed flow of charge carriers. Usually, the electric currents do not entail a considerable spin transfer because of the random orientation of electron spins. However, the charge current can be accompanied by a spin current if the electron spins are co-oriented, as happens, e.g., under injection of spin-polarized carriers from magnetic materials [1, 2] or in the optical-orientation-induced circular photogalvanic effect [3, 4]. Furthermore, there exists a possibility to create a pure spin current that is not accompanied by a net charge transfer. This state represents a nonequilibrium distribution when electrons with spin "up" propagate mainly in one direction and those with spin "down" propagate in the opposite direction. In terms of the kinetic theory, it can be illustrated by a spin density matrix with two nonzero components, namely, $\rho_{s,s}(\mathbf{k}) = \rho_{\bar{s},\bar{s}}(-\mathbf{k})$, where s and $\mathbf{k}$ are the electron spin index and the wavevector, and $\bar{s}$ means the spin opposite to s. Spin currents in semiconductors can be driven by an electric field acting on unpolarized free carriers that undergo a spin-dependent scattering and/or that propagate in a medium with spin–orbit coupling. This is the so-called spin Hall effect, wherein a pure spin transfer appears in the direction perpendicular to the electric field (see [5–8] and references therein). The spin currents can be induced as well by optical means as a result of interference of one- and two-photon coherent excitation with a two-color electromagnetic field [9] or under interband optical transitions in noncentrosymmetrical semiconductors [10].

Here, we show that pure spin currents, accompanied neither by charge transfer nor by spin orientation, can be achieved under absorption of linearly polarized or unpolarized light in semiconductor low-dimensional systems. The effect is considered here for direct interband and intersubband as well as for indirect free-carrier optical transitions in semiconductor quantum wells (QWs).

Phenomenologically, the flux of electron spins is characterized by a pseudotensor $\hat{\mathbf{F}}$, whose components F_β^α describe the flow in the β direction of spins oriented along α, with α and β being the Cartesian coordinates. In terms of the kinetic theory, such a component of the spin current is contributed by a nonequilibrium correction $\propto\sigma_\alpha k_\beta$ to the electron spin density matrix, where σ_α is the Pauli matrix. In general, the concept of spin current is uncertain in systems with spin–orbit interaction, since the spin and spin-dependent velocity cannot be determined simultaneously [11]. Mathematically, it is caused by the fact that the Pauli matrices and the velocity operator do not commute. However, this problem is overcome in most real semiconductor QWs, where spin–orbit interaction can be considered as a small perturbation. To the first order in the constant of spin–orbit coupling and within the relaxation time approximation, the pure spin current photoinduced in the conduction band is given by

$$F_\alpha^\beta = \sum_{\mathbf{k}} \tau_e \mathrm{Tr}\left[\frac{\sigma_\alpha}{2} v_\beta(\mathbf{k})\dot{\rho}(\mathbf{k})\right] \quad (1)$$

with the spin-dependent corrections being taken into account either in the velocity operator $\mathbf{v}(\mathbf{k})$ or in the photogeneration rate of the spin density matrix $\dot{\rho}(\mathbf{k})$. Here, τ_e is the relaxation time of the spin current, which can differ from the conventional momentum relaxation

¶ This article was submitted by the authors in English.

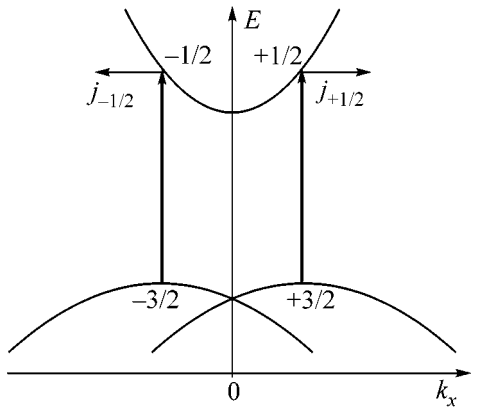

Fig. 1. Microscopic origin of pure spin current induced by interband photoexcitation. The vertical lines show the possible optical transitions.

time that governs the electron mobility. Electron–electron collisions, which do not affect the mobility, can contribute to τ_e, as happens, e.g., in the case of spin relaxation [12].

2. INTERBAND OPTICAL TRANSITIONS

The appearance of a pure spin current under direct optical transitions is linked with two fundamental properties of semiconductor QWs, namely, the *spin splitting* of the energy spectrum, which is linear in the wavevector **k**, and the spin-sensitive *selection rules* for optical transitions [13]. The effect is most easily conceivable for direct transitions between the heavy-hole valence subband *hh*1 and conduction subband *e*1 in QWs of the C_s point symmetry, e.g., in (113)- or (110)-grown QWs. In such structures, the spin component along the QW normal *z* is coupled with the in-plane electron wavevector. This leads to **k**-linear spin–orbit splitting of the energy spectrum as sketched in Fig. 1, where the heavy hole subband *hh*1 is split into two spin branches ±3/2. As a result, they are shifted relative to each other in **k** space. In the reduced-symmetry structures, the spin splitting of the conduction band is usually smaller than that of the valence band and is not shown in Fig. 1 for simplicity. Due to the selection rules, direct optical transitions from the valence subband *hh*1 to the conduction subband *e*1 can occur only if the electron angular momentum changes by ±1. It follows then that the allowed transitions are $|+3/2\rangle \longrightarrow |+1/2\rangle$ and $|-3/2\rangle \longrightarrow |-1/2\rangle$, as illustrated in Fig. 1 by vertical lines. Under excitation with linearly polarized or unpolarized light, the rates of both transitions are equal. In the presence of spin splitting, the optical transitions induced by photons of the fixed energy $\hbar\omega$ occur in opposite points of **k** space for the spin branches ±1/2. The asymmetry of photoexcitation results in a flow of electrons within each spin branch. The corresponding fluxes $\mathbf{j}_{+1/2}$ and $\mathbf{j}_{-1/2}$ are of equal strengths but opposite directions. Thus, this nonequilibrium electron distribution is characterized by the nonzero spin current $\mathbf{j}_{\rm spin} = (1/2)(\mathbf{j}_{+1/2} - \mathbf{j}_{-1/2})$ but also by a vanishing charge current, $e(\mathbf{j}_{+1/2} + \mathbf{j}_{-1/2}) = 0$.

The direction β of the photoinduced spin current and the orientation α of transmitted spins are determined by the explicit form of the spin–orbit interaction. The latter is governed by the QW symmetry and can be varied. For QWs based on zinc-blend lattice semiconductors and grown along the crystallographic direction [110] $\parallel z$, the light absorption leads to a flow along $x \parallel [1\bar{1}0]$ of spins oriented along *z*. This component of the electron spin flow can be estimated as

$$F_x^z = \gamma_{zx}^{(hh1)} \frac{\tau_e}{2\hbar} \frac{m_h}{m_e + m_h} \frac{\eta_{cv}}{\hbar\omega} I, \qquad (2)$$

where $\gamma_{zx}^{(hh1)}$ is a constant describing the **k**-linear spin–orbit splitting of the *hh*1 subband; m_e and m_h are the electron and hole effective masses in the QW plane, respectively; η_{cv} is the light absorbance; and *I* is the light intensity.

In (001)-grown QWs, the absorption of linearly polarized or unpolarized light results in a flow of electron spins oriented in the QW plane. In contrast to the low-symmetry QWs considered above, in (001) QWs the **k**-linear spin splitting of the *hh*1 valence subband is suppressed and, here, for the sake of simplicity, we assume parabolic spin-independent dispersion in the *hh*1 valence subband and take into account the spin-dependent contribution

$$H_{\rm so}^{(e1)} = \sum_{\alpha\beta} \gamma_{\alpha\beta}^{(e1)} \sigma_\alpha k_\beta \qquad (3)$$

to the electron effective Hamiltonian. Then, to the first order in the spin–orbit coupling, the components of the pure spin current generated in the subband *e*1 are derived to be

$$F_\beta^\alpha = \gamma_{\alpha\beta}^{(e1)} \frac{\tau_e}{2\hbar} \frac{m_e}{m_e + m_h} \frac{\eta_{cv}}{\hbar\omega} I. \qquad (4)$$

Hole Spin Currents

For heavy holes *hh*1, one can introduce the pseudospin description with pseudospins $\tilde{s} = \pm 1/2$ representing hole states with angular momentum ±3/2. In addition to electron spin current (4), a hole pseudospin current is induced by interband photoexcitation with linearly polarized light. In the geometry of normal incidence, the components $F_\alpha^x(hh1)$ and $F_\alpha^y(hh1)$ are given, respectively, by the real and imaginary parts of

$$F_\alpha^x + iF_\alpha^y = (\gamma_{x\alpha}^{(e1)} + i\gamma_{y\alpha}^{(e1)}) \frac{\tau_h}{2\hbar} \frac{m_e}{m_e + m_h} \frac{\eta_{cv}}{\hbar\omega} I (e_x + ie_y)^2,$$

where τ_h is the relaxation time of the hole spin current and **e** is the light polarization unit vector.

3. INTERSUBBAND OPTICAL TRANSITIONS

The intersubband light absorption in *n*-doped QW structures is a resonant process and occurs if the photon energy equals the energy spacing between the subbands. In a simple one-band model, direct optical transitions from subband $e1$ to subband $e2$ can be induced only by irradiation with the nonzero normal component e_z of the polarization vector. These transitions occur with spin conservation, $(e1, +1/2) \longrightarrow (e2, +1/2)$ and $(e1, -1/2) \longrightarrow (e2, -1/2)$, as illustrated in Fig. 2 by vertical solid lines. Due to **k**-linear spin splitting of the $e1$ and $e2$ subbands, the optical transitions induced by photons of the certain energy $\hbar\omega$ occur only at a fixed k_x, where the photon energy matches the energy separation between the subbands [4]. Similarly to the interband excitation considered in the previous section, these k_x points have opposite signs for the spin branches $\pm 1/2$. Such spin-dependent asymmetry of photoexcitation gives rise to pure spin currents in both the $e1$ and $e2$ subbands.

An interesting feature of the pure spin photocurrent induced under intersubband transitions is its spectral behavior: an increase in the photon energy $\hbar\omega$ (see Figs. 2a and 2b) leads to a shift of the points k_x that results in reversal of the spin current direction. The explicit spectral dependence of the spin photocurrent in ideal QWs depends on the specific fine structure of the energy spectrum. However, in real structures, the spectral width of the intersubband resonance is broadened and, hence, substantially exceeds the spectral width of the absorption spectrum of an ideal structure. The broadening can be taken into account assuming, e.g., that the energy separation E_{21} between the subbands varies in the QW plane. Then, to the first order in the spin–orbit coupling, the pure spin current generated under intersubband optical transitions has the form

$$F_\beta^\alpha = \frac{1}{2\hbar}(\gamma_{\alpha\beta}^{(e2)} - \gamma_{\alpha\beta}^{(e1)})\frac{I}{\hbar\omega} \times\left[\tau_{e2}\eta_{21}(\hbar\omega) + (\tau_{e1} - \tau_{e2})\bar{E}\frac{d\eta_{21}(\hbar\omega)}{d\hbar\omega}\right], \quad (5)$$

where $\gamma_{\alpha\beta}^{(e1)}$ and $\gamma_{\alpha\beta}^{(e2)}$ are the constants of the spin–orbit coupling in the $e1$ and $e2$ subbands, τ_{e1} and τ_{e2} are the corresponding relaxation times of the spin currents, $\eta_{21}(\hbar\omega)$ is the intersubband light absorbance with the inhomogeneous broadening being taken into account, and $\bar{E}$ is the mean value of the electron kinetic energy. It equals $E_F/2$ for a 2D degenerate gas with the Fermi energy E_F and k_BT for a 2D nondegenerate gas at the temperature T. Intersubband light absorption is dominated by spin-conserving optical transitions; therefore,

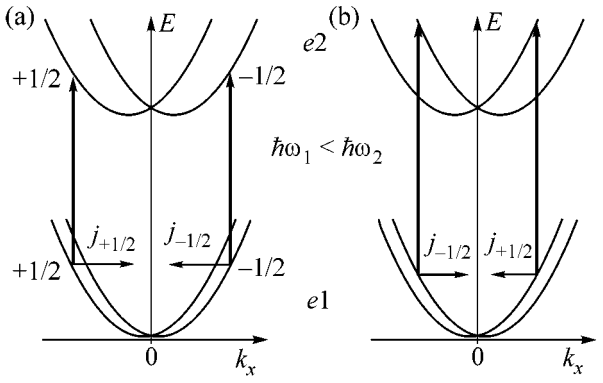

Fig. 2. Microscopic origin of pure spin current induced by intersubband photoexcitation. A change in the light frequency (a), (b) leads to reversal of the spin-current direction.

pure spin current (5) is proportional to the difference of subband spin splittings. The spectral behavior of the spin current is determined mainly by the second term in Eq. (5) and repeats the derivative of the light absorption spectrum $d\eta_{21}(\hbar\omega)/\hbar\omega$, since the relaxation time in the excited subband τ_{e2} is usually shorter than that in the lowest subband, τ_{e1}.

4. FREE-CARRIER ABSORPTION

Light absorption by free carriers, or Drude-like absorption, occurs in doped semiconductor structures when the photon energy $\hbar\omega$ is smaller than both the band gap and the intersubband spacing. Because of energy and momentum conservation, free-carrier optical transitions become possible if they are accompanied by electron scattering by acoustic or optical phonons, static defects, etc. Scattering-assisted photoexcitation with linearly- or unpolarized light also gives rise to a pure spin current. However, in contrast to the direct transitions considered above, the spin splitting of the energy spectrum leads to no essential contribution to the spin current induced by free-carrier absorption. The more important contribution comes from asymmetry of the electron spin-conserving scattering. In semiconductor QWs, the matrix element V of electron scattering by static defects or phonons has, in addition to the main contribution V_0, an asymmetric spin-dependent term [14–17]

$$V = V_0 + \sum_{\alpha\beta} V_{\alpha\beta}\sigma_\alpha(k_\beta + k'_\beta), \quad (6)$$

where **k** and **k'** are the electron's initial and scattered wavevectors, respectively. Microscopically, this contribution is caused by a structural and bulk inversion asymmetry similar to the Rashba–Dresselhaus spin splitting of the electron subbands. The asymmetry of the electron–phonon interaction results in nonequal rates of indirect optical transitions for opposite

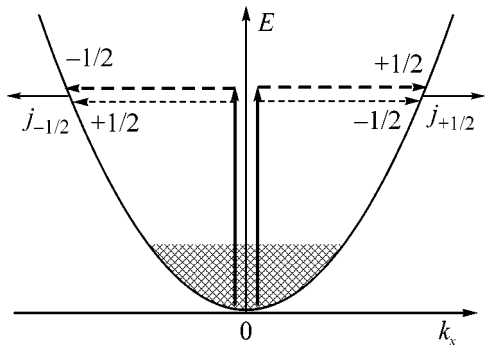

Fig. 3. Microscopic origin of pure spin current induced under light absorption by free electrons. The free-carrier absorption is a combined process involving electron–photon interaction (vertical solid lines) and electron scattering (dashed horizontal lines).

wavevectors in each spin branch. This is illustrated in Fig. 3, where the free-carrier absorption is shown as a combined two-stage process involving electron–photon interaction (vertical solid lines) and electron scattering (dashed horizontal lines). The scattering asymmetry is shown by thick and thin dashed lines: electrons with spin +1/2 are preferably scattered into the states with $k_x > 0$, while particles with spin –1/2 are scattered predominantly into the states with $k_x < 0$. The asymmetry causes an imbalance in the distribution of photoexcited carriers in each branch $s = \pm 1/2$ over the positive and negative k_x states and yields oppositely directed electron flows $\mathbf{j}_{\pm 1/2}$, which are shown by horizontal arrows. Similarly to the interband excitation considered in the previous section, this nonequilibrium distribution is characterized by a pure spin current without charge transfer.

If the photon energy $\hbar\omega$ exceeds the typical electron kinetic energy $\bar{E}$, the pure spin current induced by free-carrier light absorption is given by

$$F_x^{\alpha} = \frac{\tau_e}{\hbar}\left[\frac{V_{\alpha x}}{V_0}\left(1 + \frac{|e_x|^2 - |e_y|^2}{2}\right) + \frac{V_{\alpha y}}{V_0} e_x e_y\right]\eta_{e1} I, \quad (7)$$

where η_{e1} is the light absorbance in this spectral range. The components F_y^{α} are obtained from Eq. (7) by the replacement $x \longleftrightarrow y$.

In addition to the free-carrier absorption, the spin-dependent asymmetry of electron–phonon interaction can also give rise to a pure spin current in the process of energy relaxation of the photoexcited electrons. In this relaxation mechanism, the spin current is generated in a system of hot carriers independently of any heating means.

The mechanisms of pure spin photocurrent considered above can reveal themselves in the appearance of electric current in the presence of an in-plane magnetic field. Indeed, the application of a magnetic field results, due to the Zeeman effect, in different equilibrium populations of the subbands. The currents $\mathbf{j}_{\pm 1/2}$ flowing in the opposite directions become nonequivalent, which results in a spin-polarized net electric current [18].

Valley-Orbit Current

In addition to spin, free charge carriers can be characterized by another internal property, namely, by a well number in multi-QW structures or a valley index, l, in multivalley semiconductors. Thus, one can consider not only pure spin currents but also pure orbit-valley currents, in which case the net electric current $\mathbf{j} = \sum_l \mathbf{j}_l$ vanishes but the partial currents $\mathbf{j}_l$ contributed by carriers in the lth valley are nonzero. In carbon nanotubes, the index l runs through two equivalent one-dimensional subbands (n, K) and ($-n$, K') formed near the K and K' valleys of a graphene sheet rolled up into a cylinder, where n is the component of orbital angular momentum along the tube principal axis z [19]. In chiral nanotubes, the photoexcitation results in nonzero partial flows, $j_z(K)$ and $j_z(K')$, which have opposite signs for linearly polarized light. Another example is a GeSi/Si (111)-grown quantum-well structure. This has an overall C_{3v} symmetry and contains three equivalent two-dimensional valleys $l = 1, 2, 3$. The symmetry representing an individual valley is reduced to C_s and allows for generation of a partial in-plane photocurrent $\mathbf{j}_l$ under normal light incidence. The net electric current is absent, but one can introduce the pure valley-orbit flows $\mathbf{j} = \sum_l c_l \mathbf{j}_l$, where c_l are arbitrary nonequal coefficients.

We acknowledge helpful discussions with V.V. Bel'kov and S.D. Ganichev. This work was supported by the Russian Foundation for Basic Research, INTAS, programs of the Russian Academy of Sciences, and the Foundation "Dynasty"–ICFPM.

REFERENCES

1. R. Fiederling, M. Keim, G. Reuscher, *et al.*, Nature **402**, 787 (1999).
2. Y. Ohno, D. K. Young, B. Beschoten, *et al.*, Nature **402**, 790 (1999).
3. S. D. Ganichev and W. Prettl, J. Phys.: Condens. Matter **15**, R935 (2003).
4. S. D. Ganichev, V. V. Bel'kov, Petra Schneider, *et al.*, Phys. Rev. B **68**, 035319 (2003).
5. J. N. Chazalviel and I. Solomon, Phys. Rev. Lett. **29**, 1676 (1972).
6. A. A. Bakun, B. P. Zakharchenya, A. A. Rogachev, *et al.*, Pis'ma Zh. Éksp. Teor. Fiz. **40**, 464 (1984) [JETP Lett. **40**, 1293 (1984)].
7. Y. K. Kato, R. C. Myers, A. C. Gossard, and D. D. Awschalom, Science **306**, 1910 (2004).
8. J. Wunderlich, B. Kaestner, J. Sinova, and T. Jungwirth, cond-mat/0410295.

9. J. Hübner, W. W. Rühle, M. Klude, *et al.*, Phys. Rev. Lett. **90**, 216601 (2003).
10. R. D. R. Bhat, F. Nastos, A. Najmaie, and J. E. Sipe, cond-mat/0404066.
11. E. I. Rashba, Phys. Rev. B **70**, 161201 (2004).
12. M. M. Glazov and E. L. Ivchenko, Pis'ma Zh. Éksp. Teor. Fiz. **75**, 476 (2002) [JETP Lett. **75**, 403 (2002)].
13. *Optical Orientation*, Ed. by F. Meier and B. P. Zakharchenya (Elsevier, Amsterdam, 1984).
14. V. I. Belinicher, Fiz. Tverd. Tela (Leningrad) **24**, 15 (1982) [Sov. Phys. Solid State **24**, 7 (1982)].
15. E. L. Ivchenko and G. E. Pikus, Izv. Akad. Nauk SSSR, Ser. Fiz. **47**, 2369 (1983) [Bull. Acad. Sci. USSR, Phys. Ser. **47**, 81 (1983)].
16. N. S. Averkiev, L. E. Golub, and M. Willander, J. Phys.: Condens. Matter **14**, R271 (2002).
17. E. L. Ivchenko and S. A. Tarasenko, Zh. Éksp. Teor. Fiz. **126**, 426 (2004) [JETP **99**, 379 (2004)].
18. V. V. Bel'kov, S. D. Ganichev, E. L. Ivchenko, *et al.*, J. Phys.: Condens. Matter (in press).
19. E. L. Ivchenko and B. Spivak, Phys. Rev. B **66**, 155404 (2002).

JETP Letters, Vol. 81, No. 5, 2005, pp. 236–240. From Pis'ma v Zhurnal Éksperimental'noĭ i Teoreticheskoĭ Fiziki, Vol. 81, No. 5, 2005, pp. 297–301.

A Monte Carlo Study of the First-Order Transition in a Heisenberg FCC Antiferromagnet¶

M. V. Gvozdikova[1, 2] and M. E. Zhitomirsky[3]

[1] *Grenoble High Magnet Field Laboratory, CNRS, 38042 Grenoble, France*

[2] *Department of Physics, Kharkov National University, Kharkov, 61077 Ukraine*

[3] *Commissariat à l'Energie Atomique, DSM/DRFMC/SPSMS, 38054 Grenoble, France*

e-mail: mike.zhitomirsky@cea.fr

Received February 10, 2005

A nearest neighbor Heisenberg antiferromagnet on a face-centered cubic lattice is studied by extensive Monte Carlo simulations in zero magnetic field. The parallel tempering algorithm is utilized, which allows one to overcome a slow relaxation of the magnetic order parameter and to fully equilibrate moderately sized clusters with up to $N \simeq 7 \times 10^3$ spins. By collecting energy and order parameter histograms on clusters with up to $N \simeq 2 \times 10^4$ sites, we accurately locate the first-order transition point at $T_c = 0.4459(1)J$. © *2005 Pleiades Publishing, Inc.*

PACS numbers: 75.10.Jm, 75.50.Ee

Geometric frustration generally denotes an inability of a magnetic system to find a unique classical ground state. It arises due to a competition between exchange interactions for certain types of magnetic sublattices. The most well-known examples are triangular and kagomé lattices in two dimensions and pyrochlore and face-centered cubic (fcc) lattices in three dimensions. The intriguing behavior of geometrically frustrated magnetic materials has attracted much experimental and theoretical attention in the past decade [1]. The frustrated properties of an Ising antiferromagnet on an fcc lattice (Fig. 1) were recognized a long time ago [2]. The case of vector (Heisenberg) spins has been investigated to a lesser extent. Experimental realizations of fcc magnets include the type-I antiferromagnet UO_2 [3, 4] and the type-II antiferromagnet MnO [5].

In the present work, we investigate a nearest neighbor Heisenberg antiferromagnet on an fcc lattice described by the Hamiltonian

$$\mathcal{H} = J\sum_{\langle ij\rangle} \mathbf{S}_i \cdot \mathbf{S}_j, \qquad (1)$$

where $\mathbf{S}_i$ is a classical vector spin of unit length and J is the exchange constant. Every spin interacts with 12 nearest neighbors separated by $(\pm a, \pm a, 0)$, $(0, \pm a, \pm a)$, and $(\pm a, 0, \pm a)$. The frustrated properties of model (1) become apparent if one calculates the mean-field transition temperature $T_c^{\mathrm{MF}} = \frac{1}{3}|\min\{J_\mathbf{q}\}|$. The Fourier transform of the exchange interaction is

$$J_\mathbf{q} = 4J[\cos(q_x a)\cos(q_y a) + \cos(q_y a)\cos(q_z a) + \cos(q_z a)\cos(q_x a)]. \qquad (2)$$

The minimum is reached at $\mathbf{Q} = (\pi/a)(1, q, 0)$ with arbitrary q and all equivalent wavevectors in the cubic Brillouin zone. This set includes, in particular, the type-I antiferromagnetic structure with $\mathbf{Q}_1 = (\pi/a)(1, 0, 0)$ and the type-III ordering with $\mathbf{Q}_3 = (\pi/a)\left(1, \frac{1}{2}, 0\right)$. The type-I (type-III) structure becomes the only absolute

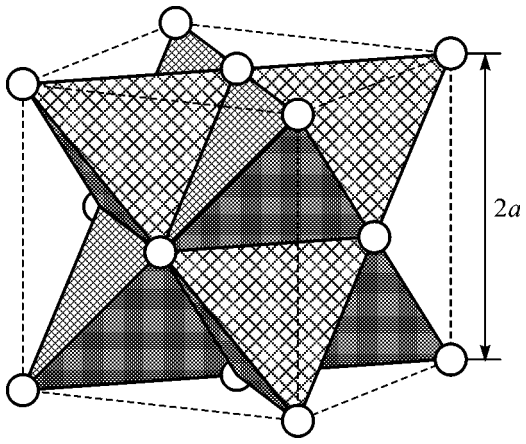

Fig. 1. Face-centered cubic lattice as a network of edge-sharing tetrahedra.

¶ This article was submitted by the authors in English.

minimum of $J_{\mathbf{q}}$ if a weak second-neighbor exchange is added to Eq. (1) with a ferromagnetic (antiferromagnetic) sign (see, e.g., [6]).

The degeneracy of the nearest neighbor model (Eq. (1)) is a consequence of the decomposition of an fcc lattice into a network of edge-sharing tetrahedra, such that every site is shared between eight tetrahedra. The classical ground-state constraint then consists in a requirement of zero total spin for every tetrahedron. This yields an infinite number of collinear and noncollinear states with different periodicities, all of which have the same classical energy. A harmonic spin-wave analysis shows that, at low temperatures, thermal fluctuations select collinear states by an "order by disorder" effect [6]. Such a result can be most easily understood by a method suggested in [7], where the effect of short-wavelength thermal fluctuations is shown to lead to an effective biquadratic exchange between neighboring spins. For classical spins on an fcc lattice, thermal fluctuations generate the following low-temperature correction to the free energy:

$$\Delta F = -\frac{T}{32}\sum_{\langle ij\rangle}(\mathbf{S}_i \cdot \mathbf{S}_j)^2. \qquad (3)$$

Such a biquadratic interaction favors collinear spin arrangement. Two examples of collinear ground states include the type-I spin structure $\mathbf{S}_i = \hat{\mathbf{e}}\cos(\mathbf{Q}_1 \cdot \mathbf{r}_i)$ and the type-III configuration $\mathbf{S}_i = \hat{\mathbf{e}}\cos\left(\mathbf{Q}_3 \cdot \mathbf{r}_i + \frac{1}{4}\pi\right)$. Additional collinear ground states are constructed from the above two configurations by selecting crystal planes (parallel to one of the cubic axes) with the Néel type of spin order and by rotating all spins in such planes by 180°. All obtained collinear states have exactly the same free energy in the harmonic approximation due to an extra gauge symmetry of the quadratic Hamiltonian [7]. Their degeneracy is lifted by anharmonicities in the spin-wave Hamiltonian—a problem that, to our knowledge, has not been considered analytically.

The finite-temperature transition of a type-I fcc antiferromagnet has been studied by the renormalization group approach [8, 9]. The absence of stable fixed points within the ϵ expansion suggests a first-order transition driven by thermal fluctuations. The above calculations have been performed for the case when the type-I structure corresponds to the absolute minimum, that is, the case of spin model (1) with a significant ferromagnetic second-neighbor exchange. In the nearest neighbor case, the anomalous contribution of thermal fluctuations is further enhanced due to extrasoft modes. Therefore, the conclusion concerning a first-order transition should remain essentially unchanged.

Numerical Monte Carlo (MC) simulations of the finite-temperature phase transition in a nearest neighbor fcc antiferromagnet have been performed by a standard single spin-flip technique [10–12]. The first-order nature of the transition at $T_c \simeq 0.45J$ was unambiguously established from the finite-size scaling of the peak in the specific heat [11] and was further supported by the energy histograms collected at the transition point [12]. As for the type of magnetic ordering at low temperatures, there is no consensus among different authors. Several early works suggested the collinear type-I antiferromagnetic structure [10, 11], though no results for the magnetic structure factor have been produced. In a subsequent, more detailed study [12], the low-temperature phase of an fcc antiferromagnet was described as "a collinear state with glassy behavior." The apparent difficulty in simulating an fcc antiferromagnet at low temperatures comes from the above-mentioned degeneracy between various collinear states, which correspond to different local minima of the free-energy functional. The collinear states transform into each other under rotation of all spins in one crystal plane. The local minima of the free energy are, therefore, separated by rather large entropy barriers $\sim L^2$, where L is a linear size of the system. A single spin-flip MC technique cannot produce appreciable shifts in the phase space between distinct collinear configurations. As a result, the spin system hardly relaxes to the absolute minimum, and the magnetic structure factor does not exhibit good averaging in a reasonable computer simulation time.

In the present work, we shall apply the novel exchange MC method [13] for simulation of a Heisenberg fcc antiferromagnet. This modification of the standard MC technique, also called parallel tempering [14], was developed for spin glasses, which are an outstanding example of hardly relaxing spin systems with numerous local minima separated by macroscopic energy barriers. In the exchange MC technique, several replicas of the spin system are simulated in parallel at a preselected set of temperatures. After a few ordinary MC steps performed on each replica, replicas that are adjacent in temperature are exchanged with a specially chosen probability [13]. The ensemble of parallel tempering thus includes two Markov processes: stochastic motion in the multidimensional phase space of the spin model and a random walk along a one-dimensional array of replicas. The second auxiliary process helps to dramatically decrease the correlation time for the main stochastic motion by repeatedly heating a given replica to high temperatures, where it quickly loses memory of the low-temperature magnetic structure. The exchange MC technique allows one to equilibrate moderately sized systems and has gained popularity in the simulation of spin glasses [15] and frustrated Ising models [16]. This method has not been applied so far to geometrically frustrated vector spin models.

We performed exchange MC simulations of model (1) on finite clusters with periodic boundary conditions and $N = 4L^3$ sites for $L = 4$, 6, 8, 10, and 12 ($N = 256$–6912). The highest temperature for the exchange MC ensemble was selected to be $T_{\mathrm{up}} = 0.75 > T_c$, where the

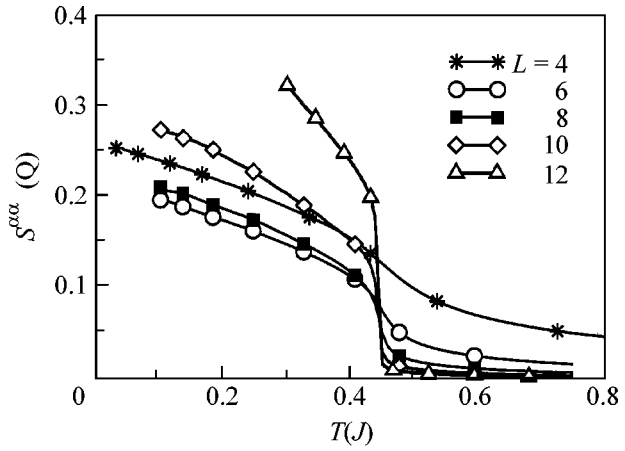

Fig. 2. Temperature dependence of the structure factor corresponding to the type-I antiferromagnetic ordering.

system equilibrates quickly with a standard MC technique. The lowest temperature in our simulations was $0.1J$. The intermediate temperatures were determined empirically starting with a geometric progression in such a way that the exchange rates for replica swaps are roughly uniform and exceed 0.1 for the largest clusters. In particular, in the vicinity of the first-order transition point, the temperature steps have to be decreased in order to avoid a bottleneck for replica drifts across T_c. In total, we employed $N_T = 72$ replicas for most cluster sizes. The MC procedure for simulation of individual replicas is the multiflipping Metropolis method (see, e.g., [11]), which includes several flipping attempts ($m = 5$ in our case) on every spin under the same local field before moving to the next spin. This method is especially suitable for an fcc lattice with a large coordination number, e.g., $z = 12$, when calculation of local fields takes a significant portion of CPU time. After sweeping twice over the whole cluster, the replica exchanges were performed. The above procedure constitutes one exchange MC step. All replicas were set in random initial configurations and equilibrated over 10^5 exchange MC steps. Measurements were performed for additional 5×10^5–4×10^6 exchange MC steps. The equilibration of various physical characteristics was checked (i) by absence of time evolution over at least half the measuring time and (ii) by comparison to results for a different set of initial replica configurations obtained by gradual annealing of a single replica from high temperatures.

During simulations of the exchange MC ensemble, the internal energy E, the specific heat, the magnetic structure factor, and the collinear order parameter were measured. Results for the internal energy and the specific heat are identical to the previous results obtained by the standard MC method [11, 12] and are not discussed here. The magnetic structure factor is given by the square of the antiferromagnetic order parameter:

$$S^{\alpha\alpha}(\mathbf{q}) = \frac{1}{N^2}\sum_{i,j}\langle S_i^\alpha S_j^\alpha\rangle e^{i\mathbf{q}(\mathbf{r}_i-\mathbf{r}_j)}, \qquad (4)$$

where $\langle\ldots\rangle$ denotes a thermal average. For $\mathbf{q} = \mathbf{Q}_3$, the structure factor exhibits a rather weak T dependence and scales as $1/N$ with increasing cluster size at all temperatures. This generally indicates an absence of the corresponding order in the thermodynamic limit at any T.

Results for the structure factor of the type-I antiferromagnetic ordering are presented in Fig. 2. Contributions from three nonequivalent wavevectors of the type-I structure are added together. Symbols are used to distinguish different curves, while lines are drawn through the actual data for $N_T = 72$ replicas. For the largest cluster, with $N = 6912$ spins, only $N_T = 39$ replicas down to $T = 0.3J$ were equilibrated. The most remarkable feature of the presented data is an *inverse* finite-size scaling at temperatures below $T_c \simeq 0.45J$: the order parameter increases with the system size. The equilibrium sublattice magnetization deduced from $S^{\alpha\alpha}(\mathbf{q})$ is still significantly smaller than 1 even at $T = 0.1J$. This is a consequence of thermally excited stacking faults, domain walls, and other defects in an ideal type-I antiferromagnetic structure. The linear size of such defects coincides with the lattice size. Their concentration, therefore, decreases with increasing system size, thus producing a significant increase of the order parameter. Unfortunately, the lattice sizes are still too small to observe an asymptotic thermodynamic behavior for $S^{\alpha\alpha}(\mathbf{q})$, though they definitely point at spin ordering with the wavevector of the type-I antiferromagnetic structure. The data for two large clusters exhibit a clear jump at the transition temperature, thus indicating the first-order transition.

Measurements of $S^{\alpha\alpha}(\mathbf{q})$ cannot distinguish between the presence of three domains of a single-q type-I structure, which is always the case for finite clusters, and a noncollinear triple-q spin state. In order to study this aspect of the magnetic ordering in an fcc antiferromagnet, we defined a collinear order parameter. This is a single-site characteristic that is insensitive to the periodicity (wavevector) of the magnetic structure but that describes instead the breaking of a spin-rotational symmetry. The collinear order parameter is given by a traceless second-rank tensor:

$$P^{\alpha\beta} = \frac{1}{N}\sum_i\langle S_i^\alpha S_i^\beta\rangle - \frac{1}{3}\delta^{\alpha\beta}. \qquad (5)$$

It vanishes for a noncollinear triple-q structure and has a nonzero value for a collinear state. In the present case, $P^{\alpha\beta}$ is a secondary order parameter: it couples linearly to a square of the primary antiferromagnetic parameter. For an XY antiferromagnet on a checkerboard lattice, $P^{\alpha\beta}$ is, however, a primary order parameter and characterizes a spin-nematic state [7].

In MC simulations, the square of order parameter (5) is measured, which is given by

$$P_{\mathrm{col}}^2 = \frac{1}{N^2}\sum_{i,j}\langle S_i^\alpha S_i^\beta S_j^\alpha S_j^\beta\rangle - \frac{1}{3}. \quad (6)$$

The corresponding results are shown in Fig. 3. Since P_{col}^2 is proportional to the fourth power of an antiferromagnetic order parameter, it does not show an appreciable jump at the first-order transition temperature. The data for the collinear order parameter exhibit a remarkable lack of finite-size scaling. This indicates that spins over the whole lattice are predominantly parallel or antiparallel to a certain direction. At $T = 0.1J$, the aligned component of spin is $\langle S^\alpha\rangle \approx 0.78$. Thus, the combination of the structure factor results (Fig. 2) and the collinear order parameter data (Fig. 3) points uniquely to the collinear type-I antiferromagnetic order in a Heisenberg fcc antiferromagnet.

Finally, we present results for the energy and the order parameter histograms (distribution functions) at the transition point. Since an fcc antiferromagnet exhibits a weak first-order transition, we find it more advantageous to perform histogram collection with a single replica instead of setting up an exchange MC ensemble. Histograms were collected utilizing a hybrid MC algorithm: three multiflipping Metropolis steps were combined with 11 overrelaxation (microcanonical) updates [17]. On average, 2×10^6 configurations were generated to build one histogram. Its accuracy was checked by comparing the final distribution function to intermediate distributions obtained with proper rescaling from 10^6 and 5×10^5 configurations. The quality of the data shown in Fig. 4 is significantly higher than in the previous work [12], which allows us to locate the transition point more precisely. The first-order nature of the transition is clearly observed from the double-peaked structure of the energy histogram (see Fig. 4). The positions of the two peaks do not change significantly with growing cluster size, while the probability for intermediate states rapidly drops with increasing L. At $T_c \approx 0.4459J$, the probability weights in the two peaks for the largest $L = 18$ cluster ($N = 23328$) differ by approximately 15%. To demonstrate the strong temperature dependence of the relative weight of the two peaks, we present in the inset of Fig. 4 the distribution functions at $T = T_c \pm 0.0001J$. The system clearly spends more time in the upper (lower) peak above (below) the transition temperature. We conclude, therefore, that the first-order transition in a Heisenberg fcc antiferromagnet takes place at $T_c = 0.4459 \pm 0.0001J$.

The distribution function for the square of the antiferromagnetic order parameter is shown in Fig. 5. The largest cluster also develops the double-peaked structure that is characteristic of the first-order transition. Smaller clusters have, however, significantly wider distributions for the magnetic structure factor, which is not

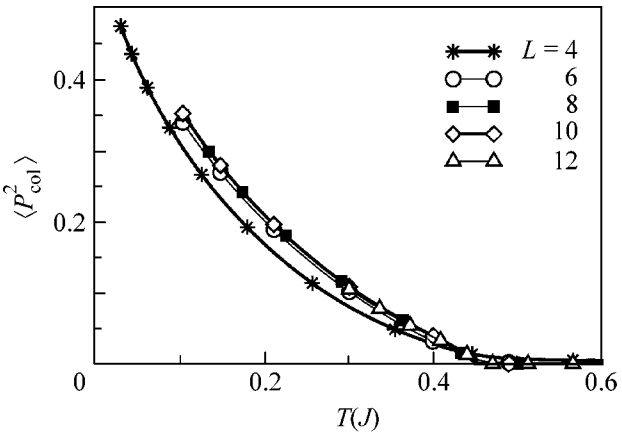

Fig. 3. Temperature dependence of the collinear (nematic) order parameter.

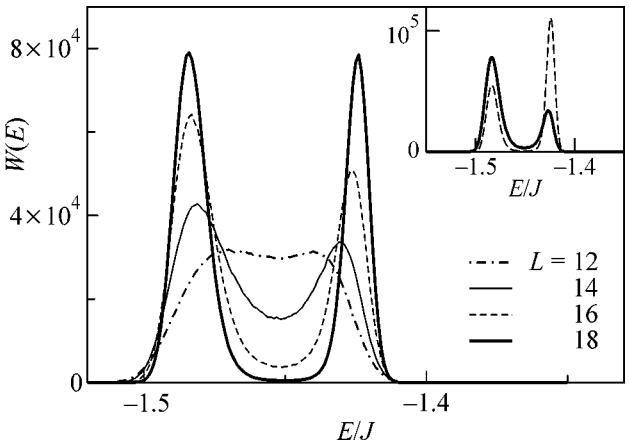

Fig. 4. Distribution function (energy histogram) for several lattice sizes at the first-order transition $T_c = 0.4459J$. Inset shows energy histograms for the largest cluster $L = 18$ ($N = 23328$) at $T = 0.4458J$ (solid line) and $T = 0.4460J$ (dashed line).

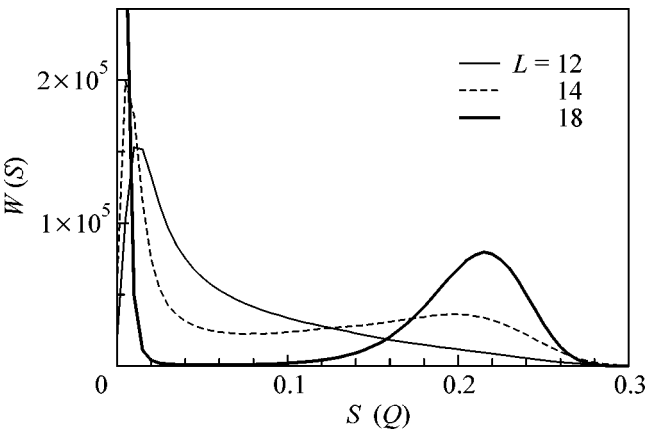

Fig. 5. Histogram for the magnetic structure factor at the first-order transition $T_c = 0.4459J$.

surprising in light of the many local minima for different collinear states. It is interesting to note that the jump of $S^{\alpha\alpha}(Q)$ at the transition point determined from the histogram for the $L = 18$ cluster (Fig. 5) is close to the jump observed for the $L = 12$ cluster in the temperature scan (Fig. 2), though the latter lattice does not exhibit any visible double-peaked structure at T_c. This indicates that, apart from the close vicinity of the transition point, the $L = 12$ cluster may be very close to the thermodynamic limit.

In conclusion, we performed Monte Carlo simulations for a finite-temperature transition in a nearest neighbor Heisenberg fcc antiferromagnet. The obtained results clearly demonstrate a first-order transition into a collinear type-I antiferromagnetic structure due to an order by disorder effect. The entropy mechanism for selecting the magnetic ordering suggests an interesting sequence of phase transitions for a weak antiferromagnetic second-neighbor exchange $0 < J' \ll T_c$. The higher temperature transition from a paramagnetic state is determined by thermal fluctuations and takes place to the type-I collinear antiferromagnetic structure. At sufficiently low temperatures $T \sim J'$, energy selection overcomes the entropy effect, and a second transition, namely, from the type-I to the type-III structure, occurs.

We are grateful to H.G. Katzgraber for helpful comments on the exchange MC method. M.E.Z. acknowledges the hospitality of the Condensed-Matter Theory Institute of Brookhaven National Laboratory during the course of this work.

REFERENCES

1. For a recent progress see *Proceedings of the Highly Frustrated Magnetism 2003 Conference*, J. Phys.: Condens. Matter **16**, S553 (2004).
2. A. Danielian, Phys. Rev. **133**, A1344 (1964); K. Binder, Phys. Rev. Lett. **45**, 811 (1980); H. Meirovitch, Phys. Rev. B **30**, 2866 (1984).
3. B. C. Frazer, G. Shirane, D. E. Cox, and C. E. Olsen, Phys. Rev. **140**, A1448 (1965).
4. J. Faber and G. H. Lander, Phys. Rev. B **14**, 1151 (1976).
5. D. Bloch, R. Maury, C. Vetter, and W. B. Yelon, Phys. Lett. A **49**, 354 (1974).
6. C. L. Henley, J. Appl. Phys. **61**, 3962 (1987).
7. B. Canals and M. E. Zhitomirsky, J. Phys.: Condens. Matter **16**, S759 (2004).
8. S. A. Brazovskii, I. E. Dzyaloshinskii, and B. G. Kukharenko, Zh. Éksp. Teor. Fiz. **70**, 2257 (1976) [Sov. Phys. JETP **43**, 1178 (1976)].
9. D. Mukamel and S. Krinsky, Phys. Rev. B **13**, 5078 (1976).
10. W. Minor and T. M. Giebultowicz, J. Phys. Colloq. **49**, C8-1551 (1988).
11. H. T. Diep and H. Kawamura, Phys. Rev. B **40**, 7019 (1989).
12. J. L. Alonco, A. Tarancón, H. G. Ballesteros, *et al.*, Phys. Rev. B **53**, 2537 (1996).
13. K. Hukushima and K. Nemoto, J. Phys. Soc. Jpn. **65**, 1604 (1996).
14. E. Marinari, *Advances in Computer Simulations*, Ed. by J. Kertész and I. Kondor (Springer, Berlin, 1998), p. 50; cond-mat/9612010.
15. H. G. Katzgraber, M. Palassini, and A. P. Young, Phys. Rev. B **63**, 184422 (2001); H. G. Katzgraber and A. P. Young, Phys. Rev. B **64**, 104426 (2001); Phys. Rev. B **65**, 214401 (2002).
16. L. W. Bernardi, K. Hukushima, and H. Takayama, J. Phys. A **32**, 1787 (1999).
17. F. R. Brown and T. J. Woch, Phys. Rev. Lett. **58**, 2394 (1987); M. Creutz, Phys. Rev. D **36**, 515 (1987).